REPORT DOCUMENTATION PAGE

Form Approved OMB NO. 0704-0188

1. AGENCY USE ONLY (Leave Blank)	2. REPORT DATE:	3. REPORT TYPE AND DATES COVERED
		Final Report 1-Jun-2003 - 31-MAY 06

4. TITLE AND SUBTITLE	5. FUNDING NUMBERS
In-Situ Study of Physical Properties And Structure Of Atmospheric Ice	DAAD190310078

6. AUTHORS	8. PERFORMING ORGANIZATION REPORT NUMBER
Victor F. Petrenko	

7. PERFORMING ORGANIZATION NAMES AND ADDRESSES	
Dartmouth College Office of Sponsored Projects 11 Rope Ferry Road, #6210 Hanover, NH 03755 -1404	

9. SPONSORING/MONITORING AGENCY NAME(S) AND ADDRESS(ES)	10. SPONSORING / MONITORING AGENCY REPORT NUMBER
U.S. Army Research Office P.O. Box 12211 Research Triangle Park, NC 27709-2211	45042-EV.1

11. SUPPLEMENTARY NOTES

The views, opinions and/or findings contained in this report are those of the author(s) and should not contrued as an official Department of the Army position, policy or decision, unless so designated by other documentation.

12. DISTRIBUTION AVAILABILITY STATEMENT	12b. DISTRIBUTION CODE
Approved for Public Release; Distribution Unlimited	

13. ABSTRACT (Maximum 200 words)

The abstract is below since many authors do not follow the 200 word limit

14. SUBJECT TERMS	15. NUMBER OF PAGES
Icing wind tunnel, Ice accretion, Liquid fraction, Water content, Adhesion strength	Unknown due to possible attachments
	16. PRICE CODE

17. SECURITY CLASSIFICATION OF REPORT	18. SECURITY CLASSIFICATION ON THIS PAGE	19. SECURITY CLASSIFICATION OF ABSTRACT	20. LIMITATION OF ABSTRACT
UNCLASSIFIED	UNCLASSIFIED	UNCLASSIFIED	UL

NSN 7540-01-280-5500

Standard Form 298 (Rev .2-89)
Prescribed by ANSI Std.
239-18 298-102

Report Title

In-Situ Study of Physical Properties And Structure Of Atmospheric Ice

ABSTRACT

This project focused on the following in situ measurements of the physical properties and structure of atmospheric ice during its growth to add to the fundamental data of atmospheric icing. (1) A new approach to determine the volumetric liquid fraction in growing atmospheric ice from in-situ measurements of capacitance and conductance was proposed. Assuming a combination model of series and parallel connections between water and ice parts of atmospheric ice, we were able to determine the time-variation of the liquid fraction from the in-situ measurements. (2) A simple technique for measuring the adhesion strength of atmospheric ice to a stainless wire during ice growth was developed and conducted. Data analysis shows that the freezing process, related to the ice temperature and the phase change of water, and the porosity of ice affect the ice adhesion. Those two factors can explain the experimental data.

List of papers submitted or published that acknowledge ARO support during this reporting period. List the papers, including journal references, in the following categories:

(a) Papers published in peer-reviewed journals (N/A for none)

Sullivan C. R., V. F. Petrenko, J. D. McCurdy, V. Kozliouk, Breaking the ice. IEEE Industry Applications Magazine, Vol. 9, No. 5, 49-54, 2003.
Ryzhkin I. A. and V. F. Petrenko, Proton Ordering in Ice at an Ice-Metal Interface, Journal of Experimental and Theoretical Physics, v. 101(2), 2005, 317-321.

Number of Papers published in peer-reviewed journals: 2.00

(b) Papers published in non-peer-reviewed journals or in conference proceedings (N/A for none)

Petrenko V. F., M. Higa, M. Starostin, and L. Deresh, Pulse Electro-thermal De-Icing, Proceedings of the 13th International Offshore and Polar Engineering Conference, pp. 435-438, Honolulu, Hawaii, USA, May 25 - May 30, 2003.

Number of Papers published in non peer-reviewed journals: 1.00

(c) Papers presented at meetings, but not published in conference proceedings (N/A for none)

Petrenko V. F., M. Higa, M, In-situ study of atmospheric ice, Proceedings of the 24th Army Science Conference, OP-06, Orland, Florida, Nov. 29 - Dec. 2, 2004.

Number of Papers not Published: 1.00

(d) Manuscripts

Petrenko V. F., M. Higa, M, In-situ study of atmospheric ice, Journal of atmospheric and ocean technology, (Submitted)
Petrenko V. F., M. Higa, M, In-situ measurements of the adhesion strength of growing atmospheric ice to stainless steel wire using a simple technique, Cold Regions Science and Technology, (In preparation)

Number of Manuscripts: 2.00

Number of Inventions:

Graduate Students

NAME	PERCENT_SUPPORTED
FTE Equivalent:	
Total Number:	

Names of Post Doctorates

NAME	PERCENT_SUPPORTED
FTE Equivalent:	
Total Number:	

Names of Faculty Supported

NAME	PERCENT_SUPPORTED
FTE Equivalent:	
Total Number:	

Names of Under Graduate students supported

NAME	PERCENT_SUPPORTED
FTE Equivalent:	
Total Number:	

Names of Personnel receiving masters degrees

NAME
Total Number:

Names of personnel receiving PHDs

NAME
Total Number:

Names of other research staff

NAME	PERCENT_SUPPORTED	
Michiya Higa	0.50	No
FTE Equivalent:	**0.50**	
Total Number:	**1**	

Sub Contractors (DD882)

Inventions (DD882)

Final Report:

In Situ Study of Physical Properties and Structure of Atmospheric ice

Proposal Number 45042-EV

Victor F. Petrenko

Thayer School of Engineering

Dartmouth College

Contents

1 Project summary

Objectives

The aim of this project is a better understanding of the physical properties and structure of atmospheric icing to produce more effective engineering response to the atmospheric icing problems, such as developments and improvements of de-icing and anti-icing devices.

It was expected that the physical properties and structure of atmospheric ice significantly vary with time during ice growth, because atmospheric icing involves the phase change from water to ice. An understanding of the time variation of the physical properties and structure of atmospheric ice is also necessary to develop and improve the anti-icing and de-icing operation systems. Whereas many studies have been performed in a variety of ways, to the best of our knowledge, most of the experimental studies are conducted after ice formation is complete, and therefore do not provide data about physical properties and structure of atmospheric ice during its dynamic phase change period.

Thus, this project focuses on the following in situ measurements of the physical properties and structure of atmospheric ice during its growth to add to the fundamental data of atmospheric icing.

Approach

Experimental techniques for investigating the physical properties and structure of atmospheric ice during its growth are the following.

- Simulation of atmospheric icing in icing wind tunnel:
  At this first stage of the project, an icing wind tunnel (Figure 1) was set up and upgraded for the purpose of

investigating the atmospheric icing under a wide range of experimental conditions.

- Capacitance and conductance measurements conducted on atmospheric ice:

Due to the large difference in electrical properties between ice and water, it is possible to obtain the liquid fraction in growing atmospheric ice by measuring the electric capacitance and conductance of atmospheric ice. To measure those parameters during ice growth, a new ice probe was designed. The ice probe was made of a copper foil having thin grid electrodes (Figure 2). The probe was manufactured using a printed circuit board technology. An advantage of this probe was that it could be made small enough not to disturb the ice growth process. And also a new data analysis method was developed to calculate the liquid fraction in the atmospheric ice from the experimental data.

- Mechanical tests conducted on atmospheric ice:

To investigate the adhesion strength of atmospheric ice during its growth, a simple technique for measuring the adhesion strength was developed. An illustration of experimental setup is shown in Figure 3. The technique simply uses several stainless wires aligned on the windward surface of the ice collector, on which ice is accumulated. The wires are able to be pulled out though holes on a wall of the test section of the icing wind tunnel. Because of simplicity, the adhesion strength of ice to wire is easy to measure at any certain moments after ice growth begins.

Significance and Army Value

Experimental data collected in the course of the proposed research will provide new and valuable information on the physical properties and structure of atmospheric ice during the

growth phase, while it still contains unfrozen liquid water. The results can then be used to improve the design of engineered structures that are subject to atmospheric icing, as well as in the development of de-icing and anti-icing devices.

Accomplishments

- Icing wind tunnel:

An icing wind tunnel is set up to simulate typical atmospheric icing. The icing wind tunnel is installed in installed in one of cold rooms of Thayer School of Engineering, Dartmouth College. The wind tunnel can operate under a wide range of experimental conditions. The maximum air speed is 35m/s in the inside of a 20 cm x 20 cm working section of the wind tunnel. The liquid water content in air (LWC) can vary from 0.1 to 5 g/m^3. The temperature can vary from 0 $^{\circ}$C to -30 $^{\circ}$C. Our studies were undertaken using this icing wind tunnel.

- Estimation of the liquid fraction in growing atmospheric ice using in situ measurements of capacitance and conductance:

A new approach to determine the liquid fraction in growing atmospheric ice from in-situ measurements of capacitance and conductance was proposed. Computer simulations and experimental data analysis of the four different connections between liquid and solid parts of atmospheric ice show that a combination of series and parallel connections is the most appropriate model for calculating the volumetric liquid fraction (W). Assuming this combination model, and using in-situ measurements of capacitance and conductance, we were able to determine the time-variation of W. An example of the results is shown in Figure 4, in which W is plotted as a function of time.

- In situ measurements of the adhesion strength of growing atmospheric ice to a stainless wire.

A simple technique for measuring the adhesion strength of atmospheric ice during ice growth was developed and conducted. The technique uses stainless steel wires aligned on the surface, on which ice accumulates. Using this technique, the adhesion strength of growing ice to wires can be measured as a function of time. The measurements were performed using an icing wind tunnel, under the conditions of liquid water content in air (LWC) from 0.3 to 2.4 g/m^3, air speeds of 10 and 20 m/s, and an air temperature of $-10\ ^{\circ}C$. The adhesion strength increases with time from about 0 and asymptotically approaches to a constant value. The adhesion strength also shows the complex LWC and air speed dependences. Figure 5 shows the time dependence of the adhesion strength of growing ice as a function of time for different LWC. Data analysis shows that the freezing process, related to the ice temperature and the phase change of water, and the porosity of ice affect the ice adhesion. Those two factors can explain well the experimental data.

Technology Transfer

- None.

Publications

Sullivan C. R., V. F. Petrenko, J. D. McCurdy, V. Kozliouk, Breaking the ice. IEEE Industry Applications Magazine, Vol. 9, No. 5, 49-54, 2003.

Petrenko V. F., M. Higa, M. Starostin, and L. Deresh, Pulse Electro-thermal De-Icing, Proceedings of the 13th International Offshore and Polar Engineering Conference, pp. 435-438, Honolulu, Hawaii, USA, May 25 – May 30, 2003.

Petrenko V. F., M. Higa, M, In-situ study of atmospheric ice, Proceedings of the 24th Army Science Conference, OP-06, Orland, Florida, Nov. 29 – Dec. 2, 2004.

Ryzhkin I. A. and V. F. Petrenko, Proton Ordering in Ice at an Ice-Metal Interface, Journal of Experimental and Theoretical Physics, v. 101(2), 2005, 317-321.

Petrenko V. F., M. Higa, M, In-situ study of atmospheric ice, Journal of atmospheric and ocean technology, (Submitted)

Petrenko V. F., M. Higa, M, In-situ measurements of the adhesion strength of growing atmospheric ice to stainless steel wire using a simple technique, Cold Regions Science and Technology, (In preparation)

Awards/Honors Received

- None

Figure 1. General view of the icing wind tunnel.
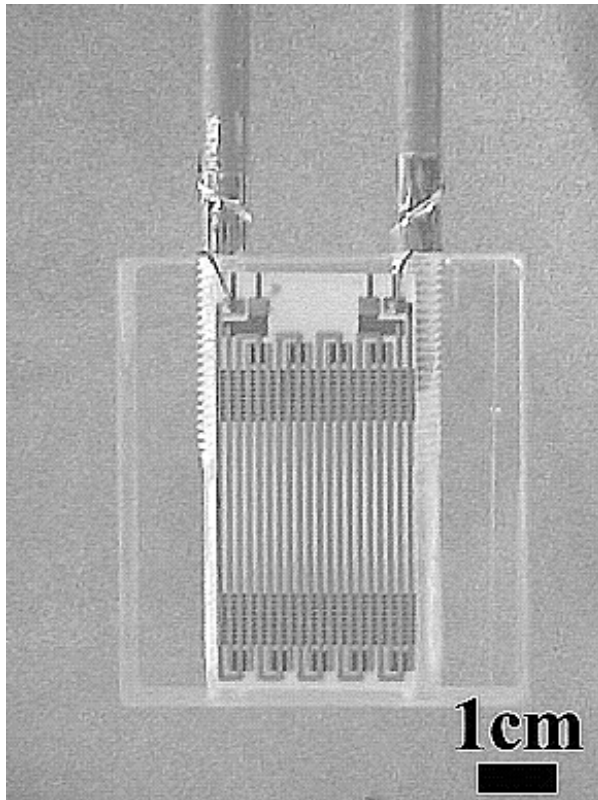
Figure 2(a). Ice probe (made of copper foil having thin grid electrodes) on the ice collector (Plexiglas). The electrodes had a width of 0.68 mm and were spaced at 0.59 mm. The electrode thickness was 0.075 mm.

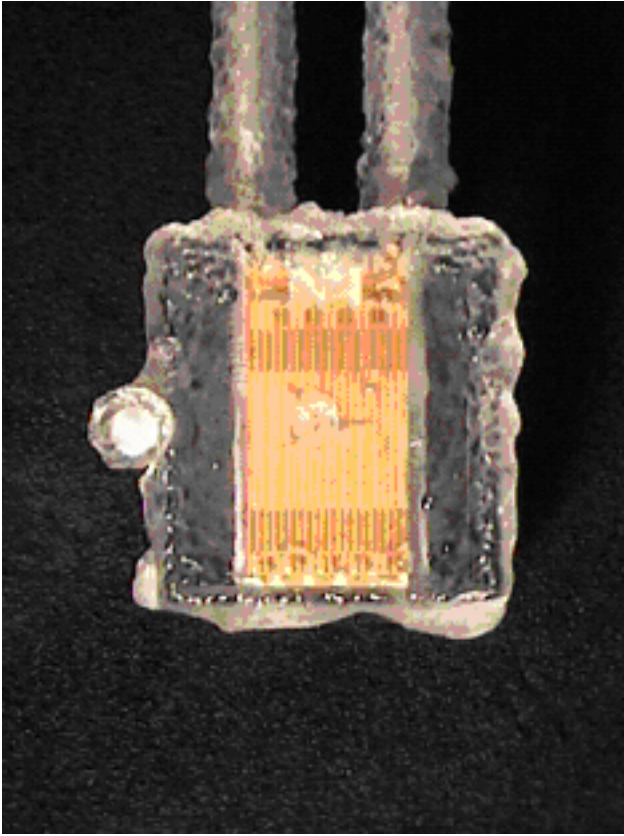Figure 2(b). An ice growth on the ice probe at T = -10 $^{\circ}$C and air speed of 33 m/s.
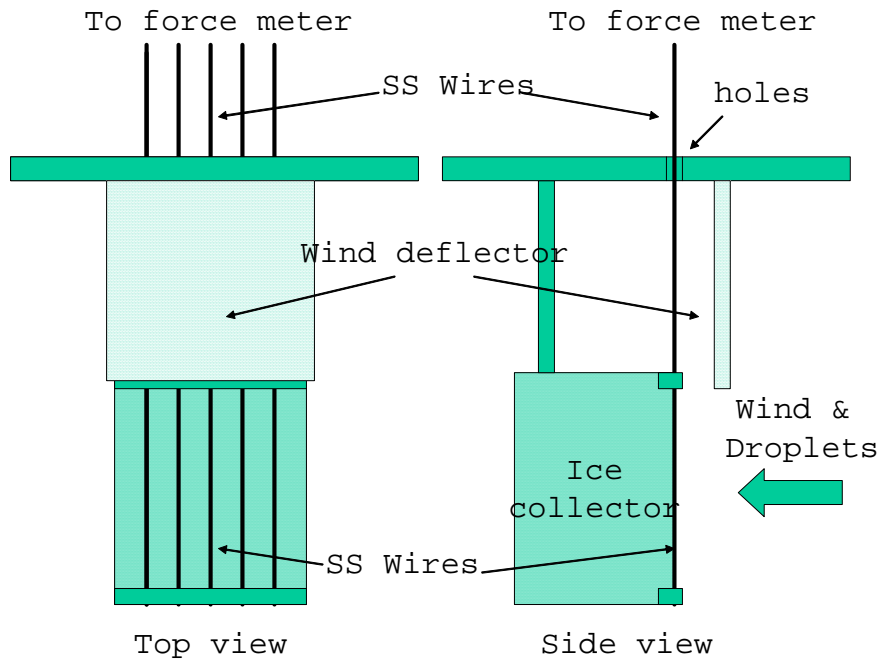
Figure 3. An illustration of experimental setup for the adhesion strength measurements.
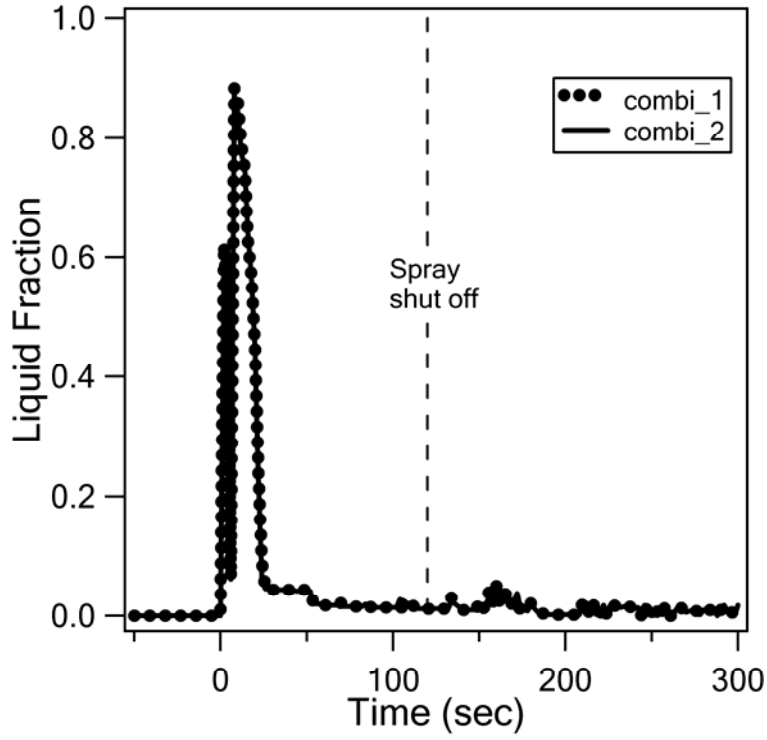
Figure 4. Time-variations of volumetric liquid fraction (W) as calculated in combination models #1 and #2. The experimental conditions: Temperature = –10 °C, air speed = 33 m/s, liquid water content in air (LWC) = 1.67 g/m^3

Figure 5. A schematic picture of the adhesion strength of growing atmospheric ice as a function of time for different LWC. The used experimental conditions: liquid water content in air (LWC) =0.3, 1.1, and 2.4 g/m^3, temperature = −10 $^{\circ}$C, air speed = 20 m/s.

2 Estimation of the liquid fraction in growing atmospheric ice using in situ measurements of capacitance and conductance

ABSTRACT

A new approach to determine the liquid fraction (W) in growing atmospheric ice from in situ measurements of capacitance and conductance was proposed. Computer simul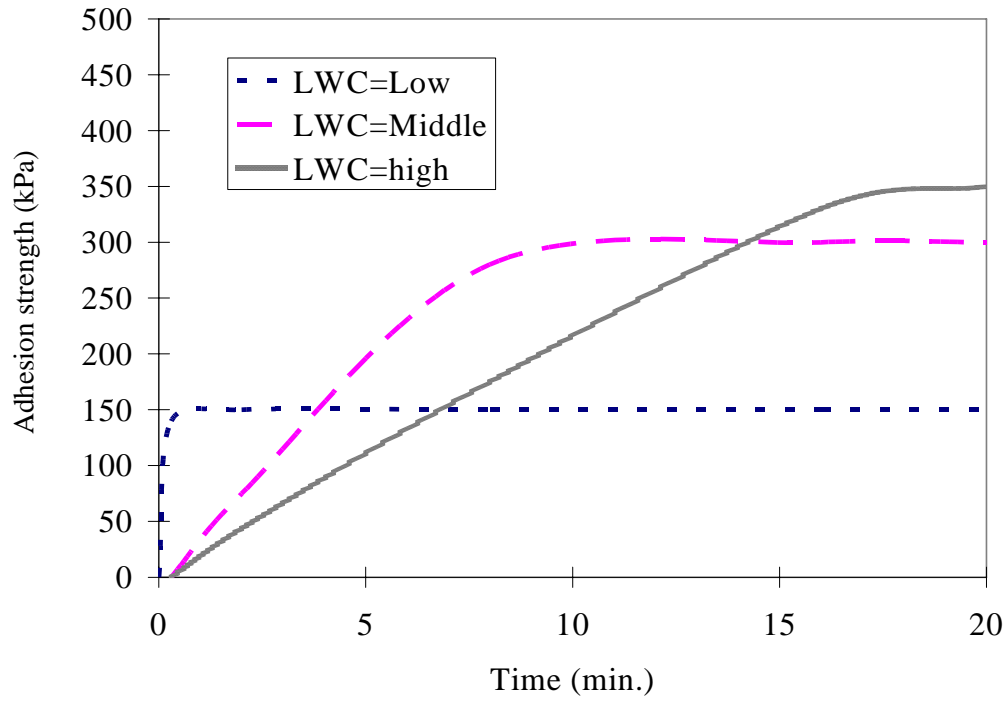ations and experimental data analysis of the four different connections between liquid and solid parts of atmospheric ice show that a combination of series and parallel connections is the most appropriate model for calculating W. Assuming this combination model, and using in situ measurements of capacitance and conductance, we were able to accurately determine the time-variation of W in growing atmospheric ice.

2.1 INTRODUCTION

The physical properties of atmospheric ice play a crucial role in the icing of structures such as aircraft, helicopters, power lines, and towers (Minsk, 1982). Since the presence of unfrozen water significantly affects these physical properties, the liquid fraction in growing atmospheric ice is one of the most important parameters to measure. While intensive theoretical and experimental studies of atmospheric ice have been done (e.g., Druez et al. 1986, Bragg et al. 1997, Lozowski et al. 2005), most were conducted after ice formation

was complete and therefore do not provide data about physical properties during the dynamic phase change period. Thus, an in-situ study of the liquid fraction is necessary to fully understand the physical properties of atmospheric ice.

Our approach for measuring the volumetric liquid fraction (W) in the growing atmospheric ice makes use of the well-known fact that ice and water differ greatly in their electrical properties such as their relative permittivity and their electric conductivity (Petrenko and Whitworth 1999). Thus, it is possible to distinguish between water and ice by measuring these electrical properties. This paper describes our approach in detail for using in-situ measurements of capacitance and conductance to calculate W.

2.2 ICING WIND TUNNEL

An icing wind tunnel was used to simulate atmospheric icing (Fig. 1). Ice was grown with a fine water-spray under turbulent-flow conditions in a 20 cm x 20 cm test section of the wind tunnel. Water droplets of distilled water were produced by a spray nozzle, manufactured by Spray Systems Co. having air cap #J73160 and fluid cap # J2050, at an air pressure of 140 kPa and a water pressure of 200-350 kPa. The icing wind tunnel is installed in installed in one of cold rooms of Thayer School of Engineering, Dartmouth College. The wind tunnel can operate under a wide range of experimental conditions. The

maximum air speed is 35m/s in the inside of a 20 cm x 20 cm working

section of the wind tunnel. The liquid water content in air (LWC) can

vary from 0.1 to 5 g/m^3. The temperature can vary from 0 $^{\circ}$C to -30 $^{\circ}$C.

2.3 ICE PROBE

Due to the large difference in electrical properties between ice

and water, it is possible to obtain the liquid fraction in growing

atmospheric ice by measuring the electric capacitance and conductance

of atmospheric ice. To measure those parameters during ice growth, a

new ice probe was designed. The ice probe was made of a copper foil

having thin grid electrodes (Fig. 2). The probe was manufactured using

a printed circuit board technology. An advantage of this probe was

that it could be made small enough not to disturb the ice growth

process. The electrodes of ice probe had a width of 0.68 mm and a

thickness of 0.075 mm. And they were spaced at 0.59 mm. A schematic

view of the ice probe is shown in Figure 3.

Using this ice probe, we measured the electrical capacitance and

conductance between probe electrodes as a function of time both during

and after ice growth. The capacitance was measured at the frequency of

200 kHz and the conductance was measured at 100 Hz. At those

frequencies, the differences in electrical properties (the

permittivity and the conductivity) between ice and water are

significant (e.g., Petrenko and Whitworth 1999). A low-frequency

14

impedance analyzer (HP4192A) was used and the maximum sampling rate in our system was 0.5 Hz.

The measured time-variation of the ice sample's capacitance (C) and conductance (G) reflect not only the liquid fraction (W) but also the sample thickness (L_s) due to the electrodes' dimensions, so that we have to separate these effects using the relationship between the capacitance of solid ice (liquid-water-free ice), (C_i) and L_s and that between the conductance of solid ice (G_i) and L_s. We determined these relationships using the electrostatic model and the conductive media DC current model from a FEMLAB software package (Comsol Inc.). This software can solve the electrostatic boundary problem and the steady electric current problem by a finite element method. We performed a simulation of the capacitance and conductance for one unit cell and calculated the total capacitance and conductance of ice sample on the whole surface of the electrodes. Here, we assumed uniform condition in the Z-direction so that the model can be treated as two-dimensional (see Fig. 4). The measured width of the electrodes and space between the electrodes are given to the unit cell (see Figure 3). Insulating boundary conditions are applied to all boundaries except the surface of the electrodes. The relative permittivity and the conductivity of solid ice are set as the values measured in our experiments for each test. Figure 4 shows an example of such simulation for the electric field in the solid ice using the electrostatic model.

Figure 5 shows the relationship between C_i and L_s and that

between G_i and L_s for solid ice obtained by the simulation. As seen in

Figs. 4 and 5, the electric field penetrates in the ice only over a

distance comparable with the inter-electrode space (≈ 0.6mm). Because

of this, the capacitance and conductance do not change much after ice

thickness exceeds that value.

2.4 RESULTS AND DISCUSSIONS

2.4.1 Time-variation of capacitance and conductance

Figure 6 shows the typical time-variations of capacitance (C)

and conductance (G) of the ice sample. These results not only show

that the electrical properties of the simulated atmospheric ice

changed significantly when the water spray was turned on and off, but

also show a complex time dependence related to the experimental

conditions. At a high rate of water flow (high air velocity times

water content in air, Fig. 6(a)) and high temperature, the sample's

capacitance monotonically decreased from a value typical for water to

one more characteristic of solid ice; while at the same time, the

sample's conductance monotonically increased (following a sharp rise

upon turning on the water spray). In contrast, at a low rate of water

flow (Fig. 6(b)), the capacitance gradually increased at a rate

closely corresponding to the increasing solid ice thickness. During

16

ice growth, however, the sample conductance quickly decreased to a level characteristic of solid ice.

Peaks seen on the time-variations of C and G in Fig.6a were typical for tests with high rate of water flow after the water spray was shut down. One possible explanation of those peaks is that unfrozen water re-enters ice/grid electrodes interface when liquid inclusions in ice ultimately freeze, perhaps, due to ice fracture.

In Figs.6a and 6b, the sample thickness effect on solid ice's capacitance and conductance obtained by the simulation are plotted with the raw data for comparison, where the simulation results are plotted as a function of time assuming the ice growth rate is constant. The data normalized to the sample thickness effect can be expressed in terms of the ratio of C/C_i and G/G_i, where C and G are the sample's capacitance and conductance respectively and C_i and G_i are the sample's capacitance and conductance obtained by a simulation. In this way, the data indicate that W approaches zero as these ratios approach one. Figure 7 shows the ratios of C/C_i and G/G_i as a function of time. It's important to remember that what is seen in Fig.7 is essentially C and G of 0.6-mm thick pre-electrode layer of ice.

2.4.2 Analysis method for calculation of liquid fraction

To determine the volumetric liquid fraction (W) in growing atmospheric ice using results on ice capacitance and ice conductance we assume some specific type of connections between frozen and

17

unfrozen parts of the ice sample. Four possible types of such connections are shown in Figure 8:

(a) Parallel connection

(b) Series connection

(c) Combination #1 of parallel and series connections

(d) Combination #2 of parallel and series connections

where X, Y, X' and Y' are fractions of water parts as shown in Fig.8 and C_w and C_i are the capacitance of the sample when it consists of all water and all ice, respectively. G_w and G_i are the conductance as well.

If we use the following notations:

$$R_c = C_w / C_i$$
$$R_g = G_w / G_i$$ (1)

W can be solved in terms of C_{total}/C_i, G_{total}/G_i, R_c, and R_g for each connection model as:

(a) Parallel connection model

$$W = X = \frac{\left(\dfrac{C_{total}}{C_i} - 1\right)}{(R_c - 1)} ,$$ (2)

$$W = X = \frac{\left(\dfrac{G_{total}}{G_i} - 1\right)}{(R_g - 1)} .$$ (3)

(b) Series connection model

$$W = Y = \frac{\left(\dfrac{C_{total}}{C_i} - 1\right) R_c}{\dfrac{C_{total}}{C_i}(R_c - 1)} ,$$ (4)

$$W = Y = \frac{\left(\dfrac{G_{total}}{G_i} - 1\right) R_G}{\dfrac{G_{total}}{G_i}(R_g - 1)} \quad .$$ (5)

(c) Combination model #1

$$W = X' + (1 - X')Y',$$ (6)

where X' and Y' can be solved by the following equations with given C_{total}/C_i, G_{total}/G_i, R_c, and R_g.

$$\frac{C_{total}}{C_i} = \frac{R_c(1 + (R_c - 1)X' - (R_c - 1)X'Y')}{R_c - (R_c - 1)Y'}$$ (7)

$$\frac{G_{total}}{G_i} = \frac{R_g(1 + (R_g - 1)X' - (R_g - 1)X'Y')}{R_g - (R_g - 1)Y'}$$ (8)

(d) Combination model #2

$$W = (1 - Y')X' + Y',$$ (9)

where X' and Y' can be solved by the following equations with given C_{total}/C_i, G_{total}/G_i, R_c, and R_g.

$$\frac{C_{total}}{C_i} = \frac{R_c(1 + (R_c - 1)X')}{R_c - (R_c - 1)Y' + (R_c - 1)X'Y'}$$ (10)

$$\frac{G_{total}}{G_i} = \frac{R_g(1 + (R_g - 1)X')}{R_g - (R_g - 1)Y' + (R_g - 1)X'Y'}$$ (11)

The ratios of both C_{total}/C_i and G_{total}/G_i are given by the data of C/C_i and G/G_i. The ratios of both C_w/C_i and G_w/G_i are constants and can be determined experimentally. Here, R_c and R_g were set as 37 and 400, respectively. They were measured at 0 °C for water and −10 °C for solid ice, respectively. Systems of Eqs. (7)-(8) and Eqs. (10)-(11) are quadratic for X' and Y' and, thus, return pairs of solutions. To

choose a right pair we applied additional criteria: $0 \leq X' \leq 1$ and $0 \leq Y' \leq 1$, and a requirement of minimum W.

Figures 9(a) and (b) show examples of the time-variations of W as calculated with assumptions of the parallel and series connection models. And Figures 10(a) and (b) show that of the combination model #1 and #2. The results show that W varies depending on the connection model chosen. The combination models #1 and #2 have the similar results of W. The reason is that the obtained X' and Y' showed the conditions of either X'<<Y' or X'>>Y' so that a term of X'Y' become smaller than terms of X' and Y'. As the results, the difference between two combination models diminished.

The results also show that W as calculated for the series model. see Figs. 9(a) and (b), with use of the conductance data is unrealistically large and is not consistent with W as calculated for the same series model with use of the capacitance data. Thus, we conclude that the series connection model is not suitable. There is a similar inconsistency of W calculated from C- and G-data for the parallel-connection model, see Figs. 9(a) and (b). But either one of two combination-connection models, see Figs. 10(a) and (b), returned consistent and reasonable values of W. For that reason, we give that model our preference. Moreover, examination of ice microstructure using thin sections cut of grown ice samples also support the assumption of mixed mode in which unfrozen water channels (grain boundaries) oriented in the electrode vicinity, see Fig.11. Figure 11

20

shows an example of thin sections of atmospheric ice at the high water

concentration and spray rates (75 km h^{-1} and 0.75 g m^{-3}) and –10 ^{o}C

obtained by our previous test. Small grains were formed at the bottom

of the ice sample and large columnar grains were formed on the top of

the small grains. There are also isolated round grains between

columnar grains. This picture indicated that we dealt with some sort

of combination of series and parallel connections of liquid and solid

regions in the ice samples. Therefore, we may conclude that a

combination of series and parallel connections of liquid and solid

regions is the most appropriate model.

2.5 CONCLUSION AND FUTURE STUDY

In order to measure volumetric liquid fraction in growing

atmospheric ice in-situ, we relied on the known differences in

electrical properties between water and ice and recorded the time-

variation of the capacitance and conductance of atmospheric ice under

a wide range of experimental conditions. We developed a data analysis

method of W for the time-variation of the samples' C and G, and then

normalized the raw data for the sample thickness effect. The liquid

fraction could then be determined from the time-variation data for

these electrical properties using a combination series and parallel

connection model.

21

In our analysis method, we ignored the dependence on temperature of the relative permittivity and conductivity (i.e., R_c and R_g). However, the time-variations of capacitance and conductance also reflect the sample's temperature changes during icing. Therefore, future study will involve taking this temperature dependence into account in order to further refine the data analysis method of the liquid fraction. We will also perform similar experiments on grids of electrodes of various dimensions to investigate how the liquid fraction varies with the distance from the interface.

2.6 APPENDIX: CAPACITANCE AND CONDUCTANCE FOR FOUR MODELS

The total capacitance of the sample (C_{total}) for each connection model can be expressed as

(a) Parallel connection model

$$C_{total} = XC_w + (1-X)C_i ,$$ (A1)

(b) Series connection model

$$C_{total} = \left(\frac{1}{C_w/Y} + \frac{1}{C_i/(1-Y)} \right)^{-1} ,$$ (A2)

(c) Combination model #1

$$C_{total} = X'C_w + (1-X')\left(\frac{1}{C_w/Y'} + \frac{1}{C_i/(1-Y')} \right)^{-1} ,$$ (A3)

(d) Combination model #2

$$C_{total} = \left(\frac{1}{C_w/Y'} + \frac{1}{(X'C_w + (1-X')C_i)/(1-Y')} \right)^{-1} ,$$ (A4)

where X, Y, X' and Y' are fractions of water parts as shown in Fig.8 and C_w and C_i are the capacitance of the sample when it consists of all water and all ice, respectively. The total Conductance of the sample (G_{total}) for each connection model can be expressed in the same way as C_{total} by replacing C_w and C_i with G_w and G_i, respectively.

2.7 REFERENCES

Bragg, M.B., S. Lee, and C.M. Henze, 1997: Heat transfer and freestream turbulence measurements for improvement of the ice accretion model. 35th AIAA Aerospace Sciences Meeting and Exhibit, Reno, NV, AIAA, Paper No.97-0053.

Druez, J., D.D. Nguyen, and Y. Lavoie, 1987: Mechanical Properties of Atmospheric Ice, Cold Region Science and Technology, **13**, 67–74.

Lozowski, E. P., M Oleskiw, R. Z. Blackmore, and A. Karev, L. Kolar, and M. Frzanch (2005) Spongy Icing Revisited: Measurements of Ice Accretion Liquid Fraction in Two Wind Tuunels, The 43rd AIAA Aerospace Siences Meeting and Exhibit, Reno, NV, 10-13 January.

Minsk, L.D., 1982: Proceedings of First International Workshop: Atmospheric icing of structures. CRREL Special Report **83–17**, 366pp.

Petrenko, V.F. and R.W. Whitworth, 1999: Physics of Ice. Oxford Univ. Press, 392pp.

2.8 FIGURE CAPTIONS

FIG. 1. Icing wind tunnel. Schematics of experimental setup. 1:
Distilled water tank (300 ml), 2: Impedance analyzer (HP4192A),
3: PC, 4: Air compressor.

FIG. 2. The copper-foil grid electrodes on the ice collector
(Plexiglas). The electrodes had a width of 0.68 mm and were
spaced at 0.59 mm. The electrode thickness was 0.075 mm.

FIG. 3. Schematic picture of ice probe's cross section. Also shows
schematic cross section of the simulation model. We assume
uniform condition in the Z-direction so that the model can be
treated as two-dimensional (see Fig. 4). ABCDEFG: outline of
unit cell, BC and FG: electrode half-widths (0.34mm), CD and EF:
electrode thickness (0.075mm), CF and DE: spacing between
electrodes (0.59mm).

FIG. 4. An example of simulation of the electric field in the ice. Ice
thickness was 1.5 mm. Arrows show the electric field in the ice.
The relative permittivity was set at 2.7. The graph represents
the unit cell of Fig. 3.

FIG. 5. Relationship between the capacitance and the ice thickness and
that between the conductance and the sample thickness obtained
by a computer simulation for solid ice. The relative

permittivity for ice was set at 2.7. The electric conductivity

of ice was set at 1×10^{-7} S m^{-1}.

FIG. 6. Typical examples of ice-sample capacitance (C) and conductance

(G) vs. time curves. The computed relation between capacitance

(C_i) and sample thickness (L_s) and that between conductance (G_i)

and L_s as calculated for solid ice are also shown for

comparison. (a) Temperature = -10 $^{\circ}$C, air speed = 115 km h^{-1},

water content in air = 1.67 g m^{-3}, and ice growth rate =

13.25×10^{-3} mm s^{-1}. (b) Temperature = -30 $^{\circ}$C, air speed = 115 km h^{-}

^{1}, water content in air = 0.25 g m^{-3}, and ice growth rate =

6.39×10^{-3} mm s^{-1}.

FIG. 7. An example of the time-variations of C/C_i and G/G_i in growing

atmospheric ice. (a) The same run as in Fig.6a. (b) The same

run as in Fig.6b.

FIG. 8. Connection models between water and ice parts in the

atmospheric ice.

FIG. 9. Time-variations of W as calculated in parallel and series

connection models. (a) The same run as in Fig.6a. (b) The same

run as in Fig.6b.

Fig. 10. Time-variations of W as calculated in combination model #1

and #2. (a) The same run as in Fig.6a. (b) The same run as in

Fig.6b.

FIG. 11. Thin section of atmospheric ice at high water rate conditions

(75 km h^{-1} and 0.75 g m and −10 $^{\circ}$C. Air flow was parallel to
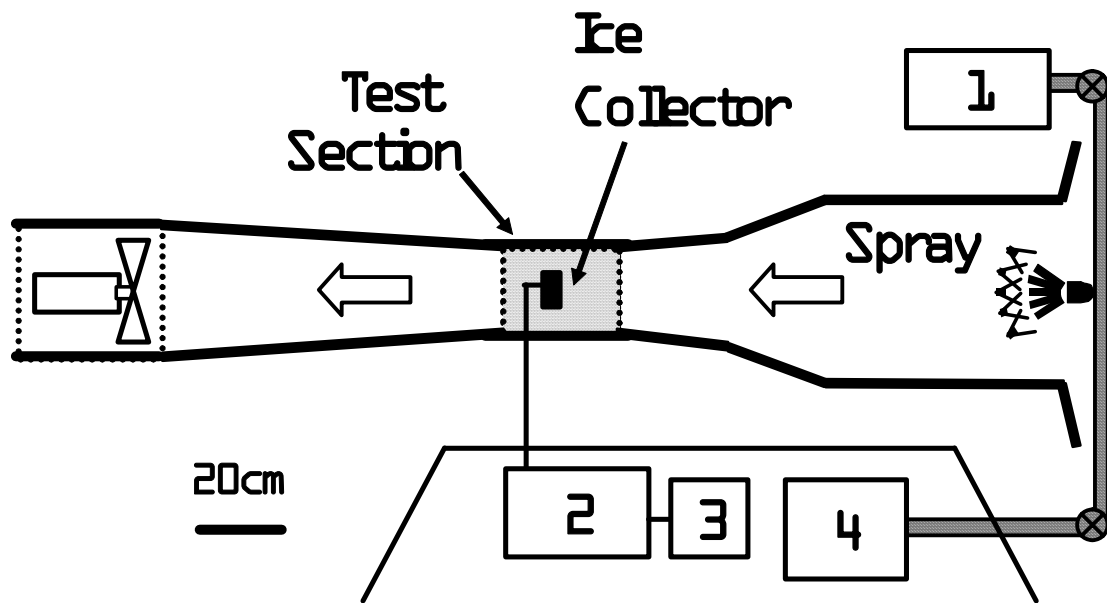
elongating column grains.

Fig.1

FIG. 1. Icing wind tunnel. Schematics of experimental setup. 1: Distilled water tank (300 ml), 2: Impedance analyzer (HP4192A), 3: PC, 4: Air compressor.
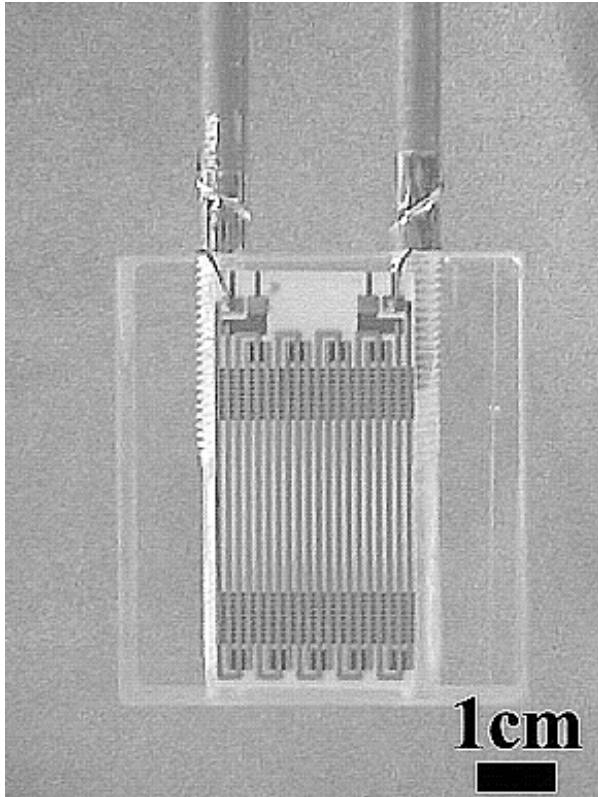
Fig.2

FIG. 2. The copper-foil grid electrodes on the ice collector
(Plexiglas). The electrodes had a width of 0.68 mm and were spaced at
0.59 mm. The electrode thickness was 0.075 mm.
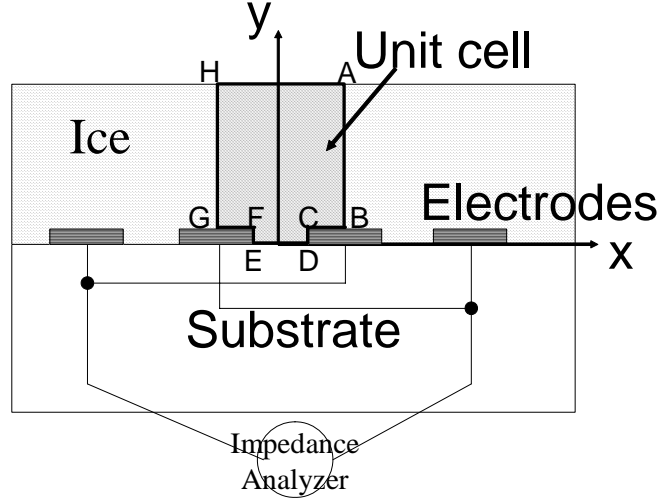
Fig.3

FIG. 3. Schematic picture of ice probe's cross section. Also shows schematic cross section of the simulation model. We assume uniform condition in the Z-direction so that the model can be treated as two-dimensional (see Fig. 4). ABCDEFG: outline of unit cell, BC and FG: electrode half-widths (0.34mm), CD and EF: electrode thickness (0.075mm), CF and DE: spacing between electrodes (0.59mm).
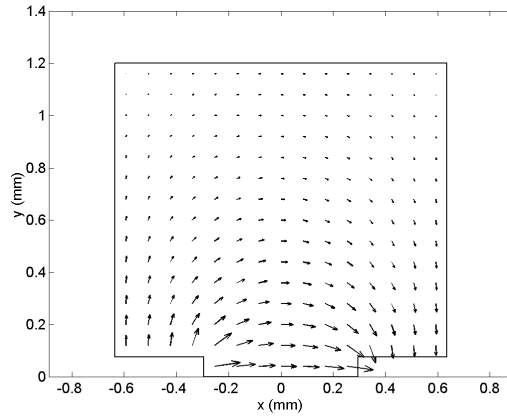
Fig.4

FIG. 4. An example of simulation of the electric field in the ice. Ice thickness was 1.5 mm. Arrows show the electric field in the ice. The relative permittivity was set at 2.7.
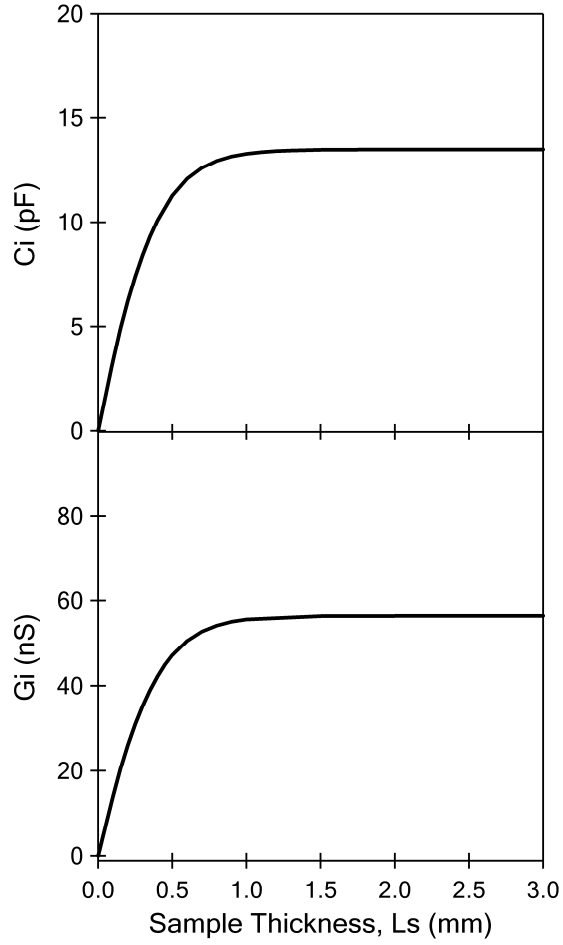
Fig.5

FIG. 5. Relationship between the capacitance and the sample thickness and that between the conductance and the sample thickness obtained by a computer simulation for solid ice. The relative permittivity for ice was set at 2.7. The electric conductivity of ice was set at 1×10^{-7} S m^{-1}.

Fig.6(a)

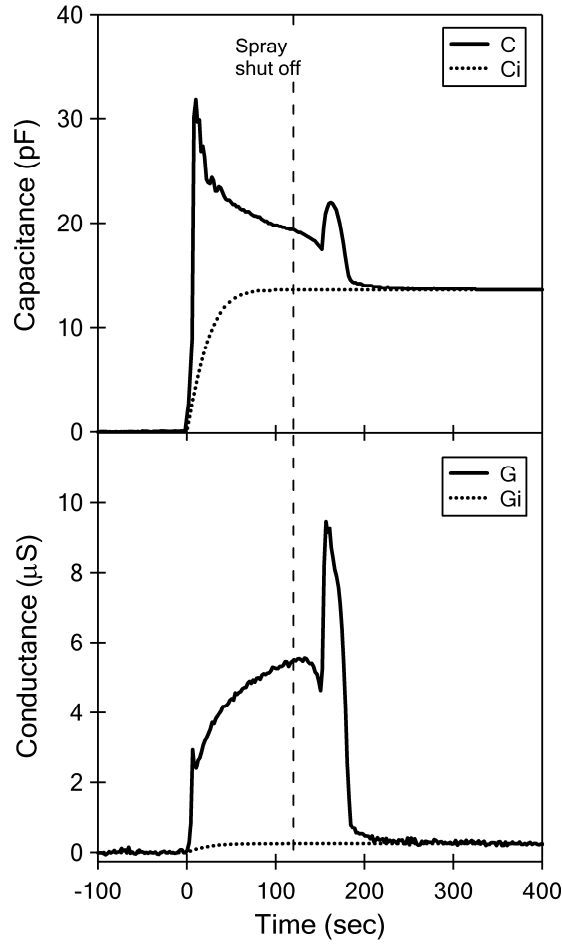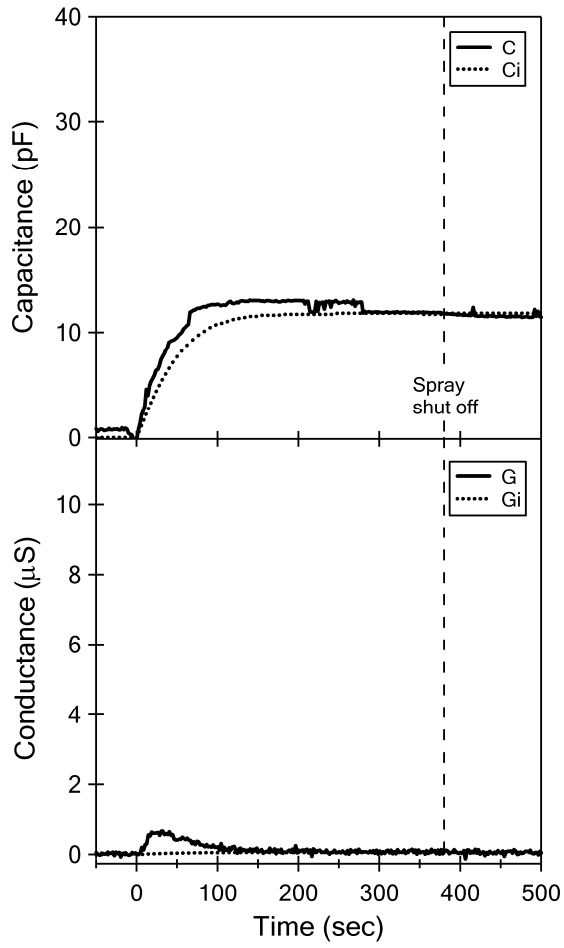FIG. 6. Typical examples of ice-sample capacitance (C) and conductance (G) vs. time curves. The computed relation between capacitance (C_i) and sample thickness (L_s) and that between conductance (G_i) and L_s as calculated for solid ice are also shown for comparison. (a) Temperature = –10 $^{\circ}$C, air speed = 115 km h^{-1}, water content in air = 1.67 g m^{-3}, and ice growth rate = 13.25x10^{-3} mm s^{-1}. (b) Temperature = –30 $^{\circ}$C, air speed = 115 km h^{-1}, water content in air = 0.25 g m^{-3}, and ice growth rate = 6.39x10^{-3} mm s^{-1}.

Fig.6(b)

(b) Temperature = −30 $^{\circ}$C, air speed = 115 km h^{-1}, water content in air = 0.25 g m^{-3}, and ice growth rate = 6.39x10^{-3} mm s^{-1}.
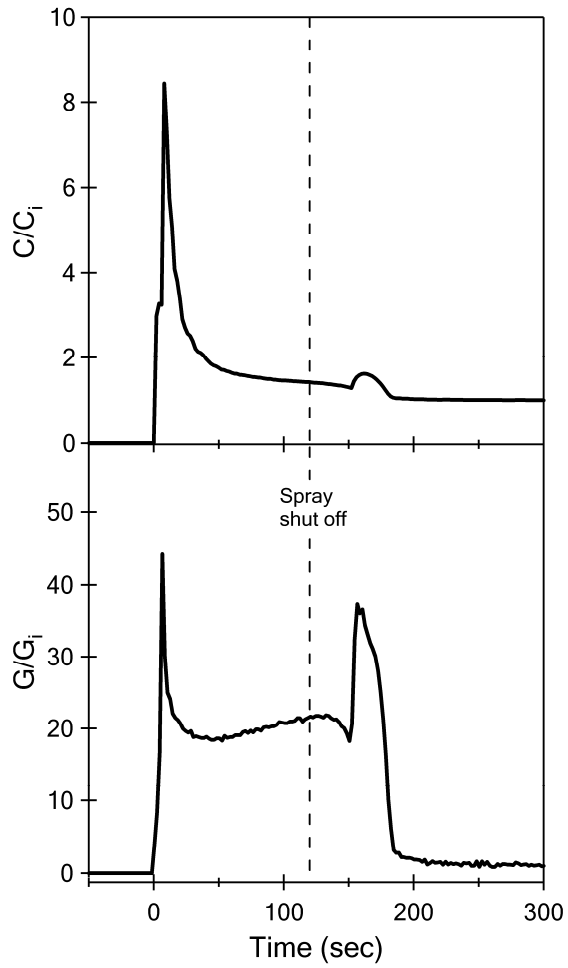
Fig.7a

FIG. 7. An example of the time-variations of C/C_i and G/G_i in growing atmospheric ice. (a) The same run as in Fig.6a. (b) The same run as in Fig.6b.
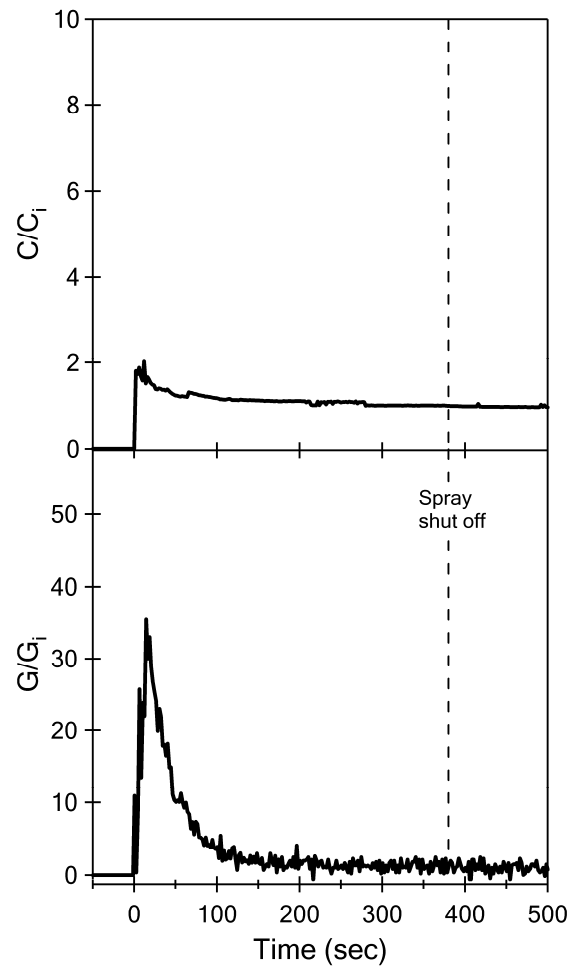
Fig.7b

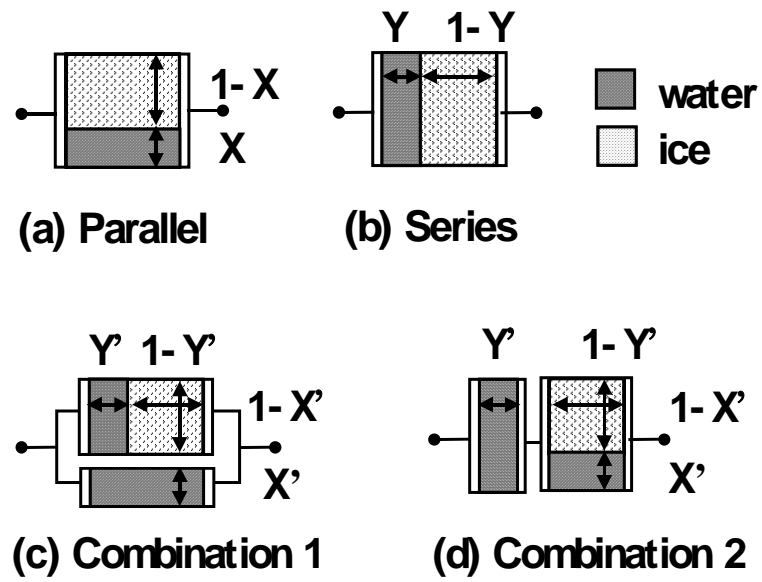
FIG. 7. (b) The same run as in Fig.3b.

Fig.8

FIG. 8. Connection models between water and ice parts in the atmospheric ice.
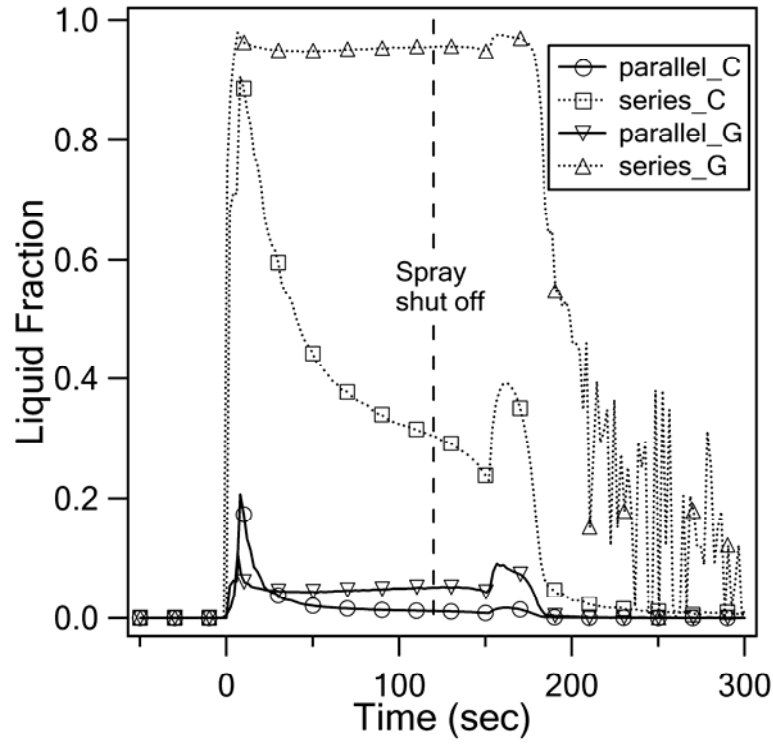
Fig.9(a)

FIG. 9. Time-variations of W as calculated in parallel and series connection models. (a) The same run as in Fig.6a. (b) The same run as in Fig.6b.
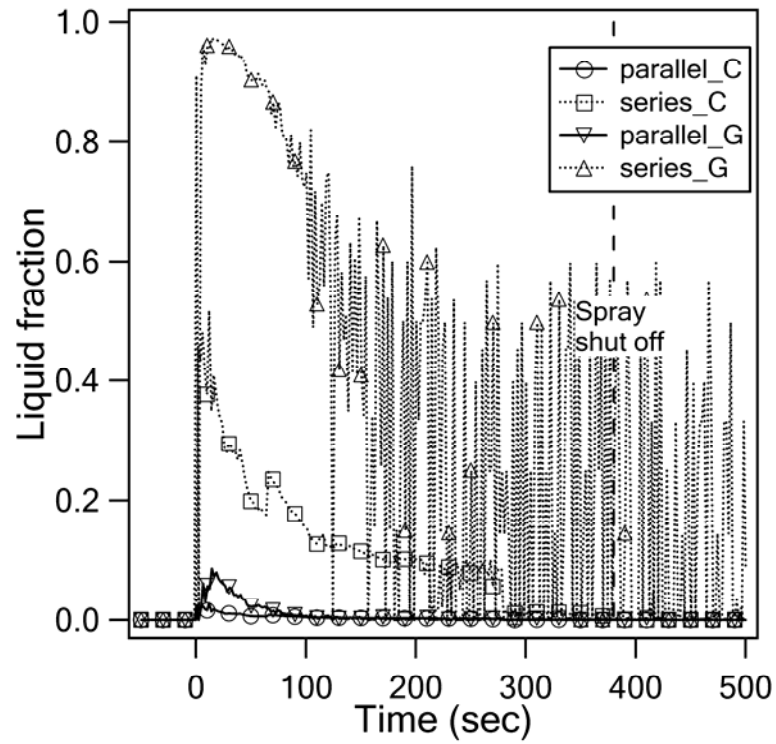
Fig.9(b)

Fig.9. (b) The same run as in Fig.6b.

Fig.10(a)
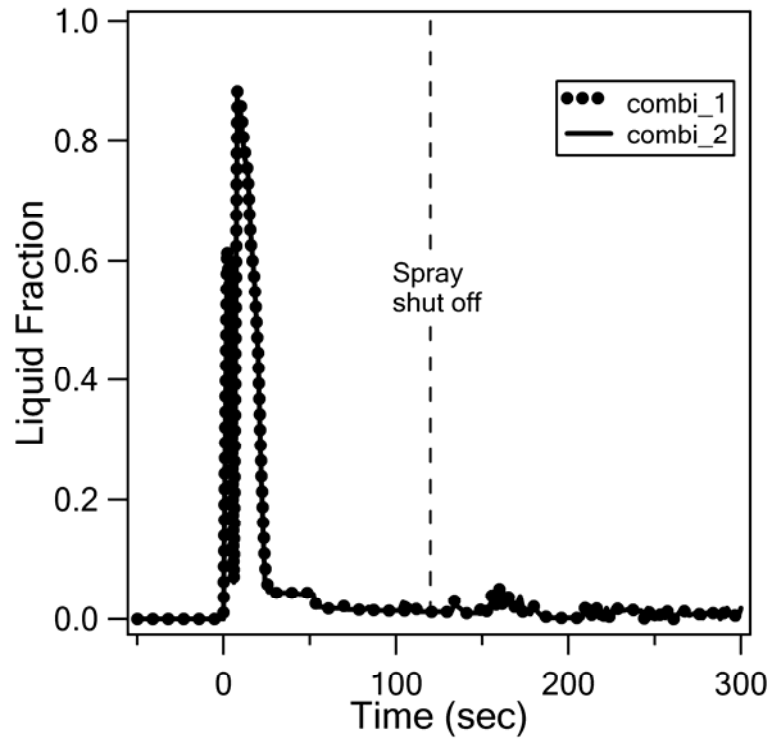

Fig. 10. Time-variations of W as calculated in combination model #1 and #2. (a) The same run as in Fig.6a. (b) The same run as in Fig.6b.

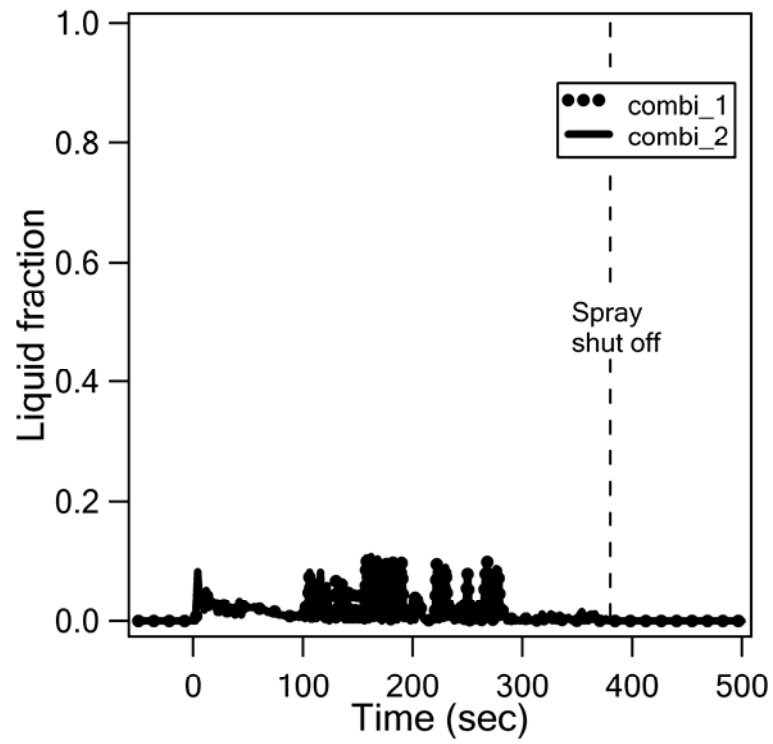**Fig. 10(b)**

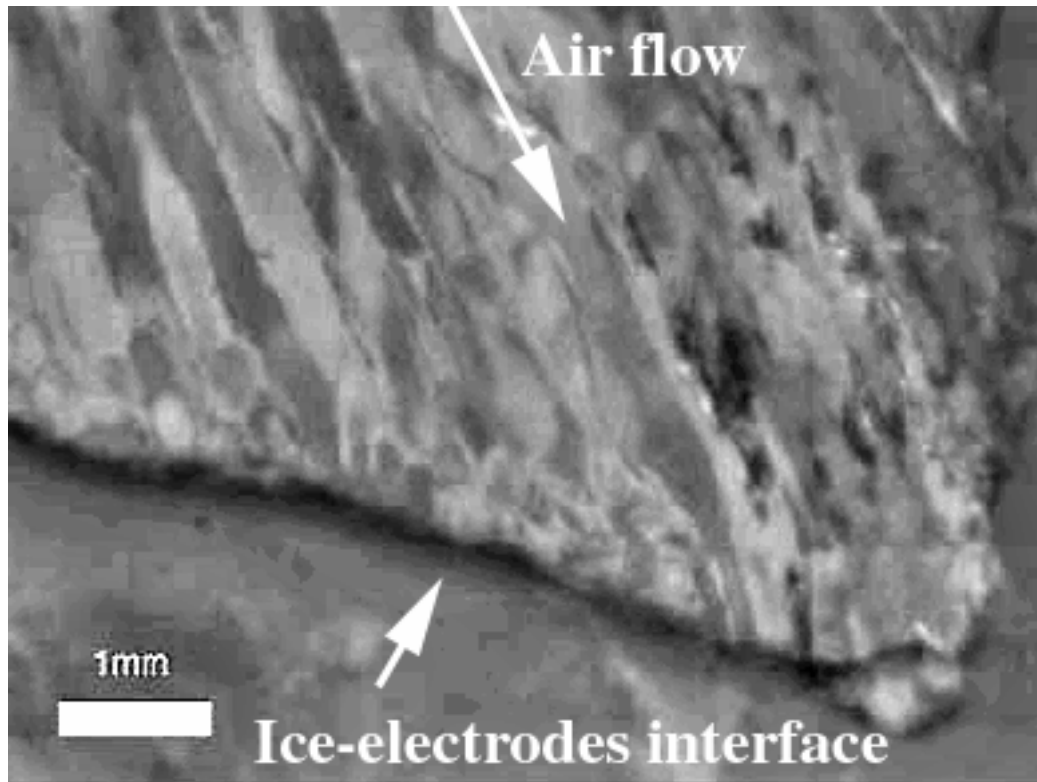Fig. 10. (b) The same run as in Fig.6b.

Fig.11

FIG. 11. Thin section of atmospheric ice at high water rate conditions (75 km h^{-1} and 0.75 g m^{-3}) and −10 $^{\circ}$C. Air flow was parallel to elongating column grains.

3 In situ measurements of the adhesion strength of growing atmospheric ice to a stainless steel wire

Abstract

A simple technique for measuring the adhesion strength of atmospheric ice during its growth is described. The technique uses stainless steel wires aligned on the surface, on which ice accumulates, and measures the adhesion strength of ice to wires during ice growth using a force sensor. The measurements are performed using an icing wind tunnel, under the conditions of liquid water content (LWC) from 0.3 to 2.4 g/m^3, air speeds of 10 and 20 m/s, and an air temperature of –10 $^{\circ}$C. Using this technique, the adhesion strength of growing ice can be measured as a function of time. The adhesion strength increases with time from about 0 and it becomes close to a constant value. It also shows the complex LWC and air speed dependences. The freezing process, related to the ice temperature and the phase change of water, and the porosity affect the ice adhesion. Those two factors can explain well the experimental data.

3.1 Introduction

Atmospheric icing on surfaces of structures and transportations is commonly observed in a variety of cold environments. The atmospheric ice can intensively accumulate on the surfaces, depending

43

the environmental conditions. However, it is very difficult to remove

expect by melting due to this strong adhesion of ice to other

material. Because of this, it can cause serious icing problems

impacting on human life and economy. To prevent the icing problems,

mechanical de-icing techniques have been endeavored to develop by many

engineers. Whereas, the development of the techniques requires

knowledge of the physical properties of the atmospheric ice,

especially, the adhesion strength of atmospheric ice to substrate

material, few studies on atmospheric ice adhesion has been performed

(e.g., Druez et al. 1986, Javan-Mashmool et al. 2006). Thus knowledge

of the adhesion strength of atmospheric ice is necessary to any step

aiming to develop new de-icing technologies.

Whereas the measurements of the adhesive strength of atmospheric

ice have been reported (e.g., Druez et al. 1986), most were conducted

after ice formation was complete. Recent studies in atmospheric icing

have shown that a large portion of the unfrozen water is trapped in

the ice formation. For example, according to Lozowski et al. (2005),

ice accretions formed under certain in-flight conditions can contain

unfrozen liquid water in amount up to 30%. Those results suggest that

the physical properties of ice after its formation are different from

those measured during its formation phase since presence of unfrozen

liquid water can drastically change the physical properties of ice. A

better understanding of the time dependence of the adhesive strength

during ice growth will provide more effective engineering response to

anti-de-icing operation systems. Therefore, the measurements of the adhesion strength during ice growth are necessary.

In this paper, a new technique for measuring the adhesion strength during ice growth is described and the time, LWC and air speed dependences of the adhesion strength are discussed.

3.2 Proposed technique

A technique uses wires aligned on the surface, on which ice accumulates, and measures the adhesion strength of ice to wires during ice growth using a force sensor. Figure 1 shows an illustration of experimental setup. Ice collector made of Plexiglas (6x5 cm^2, 5cm of thickness) was used as a substrate where ice was accumulated. Five wires were aligned on the windward surface of the ice collector at regular intervals (0.5-0.7 cm). Here, A 0.5 mm diameter stainless steel wire was used, whose maximum loading was large enough to measure the adhesion strength of ice. The ends of wires were attached to the collector's surface using a mending tape. The wires are able to be pulled out though holes on a wall of the test section. The wires were carefully cleaned with alcohol, dried and finally placed in the test section. The wind deflector was used for preventing the ice growth on the upper ends of the wires.

The measurement procedure was the following. At a certain moment after ice formation begins, we slowly pulls a wire out from the ice

and the recorded the time and the maximum tensile force. The tensile force was measured using a force meter. The adhesion strength of ice to the wires was calculated for the measured tensile force considering the icing surface area of wires. A 0.5 mm diameter stainless steel wire was used here, whose maximum loading was large enough to measure the ice adhesion.

3.3 Icing wind tunnel

The experiments were performed using a wind tunnel installed in one of cold rooms of Thayer School of Engineering, Dartmouth College. The wind tunnel has a 20 cm x 20 cm test section, in which atmospheric ice is produced by a fine water-spraying nozzle under turbulent-flow conditions. The distance between the spray nozzle and the test section is 1.4m. Water droplets are produced by a spray nozzle, manufactured by Spray Systems Co. having air cap #J73160 and fluid cap #J2050. Air flow was supplied to the air cap from a compressor using air pressure of 140 kPa, and de-ionized water was supplied to the fluid cap from a water tank using a water pressure of 200-350 kPa. The measurements were performed at liquid water content in air (LWC) ranging from 0.3 to 2.4 g/m^3, at air velocities of 10 and 20 m/s and at an air temperature of -10°C.

3.4 Results and discussions

3.4.1 Effect of freezing process on ice adhesion

Figure 2 shows an example of the adhesion strength of growing ice as a function of time. Those measurements were performed at LWC of 1.1 +/- 0.3 g/m^3, an air speed of 20 m/s, and a temperature of -10 $^\circ$C. This figure shows that the adhesion strength significantly depends on time.

There are three possible factors causing the time dependence of the adhesion strength of growing ice. One possible factor might be the porosity. However, we can suppose that the porosity does not change during ice growth and the physical properties of air do not change under our experimental conditions. Therefore, the porosity cannot explain this time dependence. The second factor is the freezing process. The freezing process should vary with time due to the time variation of the ice temperature and the phase change from water to ice. The last factor is the wire size. The adhesion strength may increase with time because the ice thickness increases with time. However this effect does not reflect the ice's material properties so that this effect must be separated from the data.

To separate the wire size effect from the data and evaluate the effect of freezing process, we introduce a dimensionless parameter, Rt. It is defined as the adhesion strength of growing ice relative to that of "frozen ice" for the same ice thickness and made under the same experimental conditions. It should be noted that we are using the term "frozen ice" as the ice that has been frozen completely and its

47

temperature has reached the same value as the air temperature. From the definition of Rt, the normalization cancels out the wire size effect.

To calculate Rt, the three parameters must be known: the adhesion strength of growing ice, the thickness of growing ice, and the adhesion strength of frozen ice for the same thickness. The first parameter is obtained from the in situ measurements directly. However, as a matter of fact, the last two parameters are difficult to measure directly, so that those two are calculated as following. For the thickness of growing ice, we convert the time to the thickness assuming that the ice growth rate is a constant. In this case, the growth rate can be calculated from the final ice thickness and its growth time. Those two are easy to measure. For the adhesion strength of frozen ice, we measure the adhesion strength of frozen ice as a function of thickness under the same experimental conditions after the water supply was shut down and ice was given enough time to freeze completely (provide that time).

Figure 3 shows an example of the adhesion strength of frozen ice measured at the same conditions as in Figure 2. The adhesion strength of frozen ice seems to increase with the increase of ice thickness slightly. This trend is explained by the wire size effect on the measurements as we discussed before. The trend line shown in figure 2 was used for calculation of Rt.

Figure 4 shows Rt as a function of time for data in Figure 2. Rt increases with time. It shows about 0 at the beginning of ice growth (e.g., Rt is 0.15 at 1 minute) and it becomes close to unity. That means that the freezing process is more effective in weakening the adhesion strength at the beginning of ice growth but this effect gradually diminishes. Therefore, we conclude that the freezing process is the major factor that causes the time dependence of the adhesion strength of growing ice. In the following sections, we will discuss the LWC and air speed effects on Rt.

3.4.2 Effect of LWC on dimensionless parameter Rt

In order to explore the effect of LWC on Rt, two more series of experiments were performed: one at $0.3+/-0.3$ g/m^3 runs and the second at $2.4 +/-0.3$ g/m^3 runs under otherwise identical conditions. (the air speed of 20 m/s and air temperature of -10 ^{o}C as in Figure 2 were maintained.) Figure 5 shows the adhesion strength as a function of time for all data series of growing ice and Figure 6 shows the adhesion strength as a function of ice thickness for all data series of frozen ice. The same analysis was performed and the results are shown in Figure 7 in which Rt is plotted as a function of time. It is noted that, in the case of the lowest LWC (0.3 g/m^3 runs), we assumed that Rt was unity during ice formation because there was no significant difference in the adhesion strength between accumulating ice and frozen ice as shown in Figure 8. It means that freezing

49

process under the lowest LWC is complete as soon as droplets stick to the surface.

Comparison of the three data series in Figure 7 shows the following. Rt becomes smaller with the increase of LWC. For example, Rt at the highest LWC (2.4 g/m^3 runs) is about 0.05 at 2 minutes and 0.25 even if 8 minutes while Rt at the lowest LWC (0.3 g/m^3 runs) is unity. Therefore, we conclude that the presence of unfrozen water in ice is the major factor reducing ice adhesion strength. As we have demonstrated above, the fraction of unfrozen water increases with increasing LWC in air.

3.4.3 Effect of air speed on dimensionless parameter Rt

In order to explore the effect of air speed on Rt, two series of experiments were performed: one at 20 m/s run, already shown in Figure 2, and the second at 10 m/s run at the same air temperature of -10 $^{\circ}$C. In particular, the same liquid flux of about 23 g/m^{2}s between the two sets of measurements was maintained, so that, while the LWC was 1.1+/-0.3 g/m^3 at 20 m/s (giving 22+/-6 g/m^{2}s), it was 2.4+/-0.3 g/m^3 at 10 m/s (giving 24+/-3 g/m^{2}s). Figure 9 shows the adhesion strength as a function of time for all data series of growing ice. Figure 10 shows the adhesion strength as a function of ice thickness for all data series of frozen ice. To explore the effect of air speed on Rt, the same analysis as in the previous section was performed and the results are shown in Figure 11 in which Rt is plotted as a function of time.

50

Comparing the above two data series, we find that Rt becomes larger with the increase of air speed. From the air speed dependence of Rt, we conclude that the water freezing rate was lower at the lower air speed, as could be expected due to a lower expected heat convection coefficient at that air speed.

3.4.4 Effect of porosity on ice adhesion

As seen in Figures 6 and 10, the adhesion strength of frozen ice increases with either the increase of LWC or the decrease of air speed. Those dependences can be explained by either an effect of the LWC and air speed dependences of the porosity because the material strength decreases with the increase of porosity. And moreover, the porosity of atmospheric ice, in general, varies with LWC and air speed.

From the naked eye observation of the frozen ice, we notice that ice porosity, in contrast to the adhesion strength, tends to decrease with either the increase of LWC or the increase of air speed. Therefore, we conclude that the LWC and air speed dependences of the adhesion strength of frozen ice can be explained by the variations of LWC and air speed on ice porosity.

Figure 6 and 10 also show that the adhesion strength of frozen ice is almost independent of thickness if the thickness is large enough in comparison with the wire size. That supports the assumption that the porosity does not change during and after ice growth.

51

Therefore, we conclude that the porosity affects the adhesion strength of the growing ice as well as that of the frozen ice.

Our experimental results also suggest that the weakening of the adhesion strength due to the porosity becomes dominant after a certain time, at which the weakening due to the freezing process becomes relatively insignificant.

3.4.5 Combined effect of LWC and air speed on ice adhesion

From the previous discussion about the porosity effect, we, intuitively, expect that the adhesion strength of growing ice increases with either the increase of LWC or the decrease of air speed. However, this intuition is not consistent with the trends seen in Figure 5, in which the adhesion strength at 0.3 g/m^3 is larger than that at 1.1 g/m^3 but the relation becomes opposite after about 4 minutes.

Those complex trends can be explained by a combined effect of the freezing process and the porosity on the adhesion strength. Let us recall the time dependence of both factors. The porosity is independent of time, while the freezing process significantly depends on time. Because of this difference, the freezing process is the dominant factor in weakening the adhesion strength at the beginning of ice growth but it gradually diminishes and then the porosity becomes the dominant factor. Let us also recall the LWC and air speed dependences of both factors. The freezing process becomes more

52

effective in weakening the adhesion strength with either the increase of LWC or the decrease of air speed, while the porosity factor becomes less effective as the porosity decreases with either the increase of LWC or the decrease of air speed. As the results, the adhesion strength decreases with either the increase of LWC or the decrease of air speed in the beginning of ice growth, however, that became opposite after a certain time. A schematic picture of those trends is shown in Figure 12, in which the adhesion strength is plotted as a function of time for different LWC. Those trends are consistent with the trends seen in Figure 5. Therefore, we conclude that the combined effect of the freezing process and porosity factors can well explain the LWC and air speed dependence of the adhesion strength of growing ice.

3.5 Conclusion

In this paper, we presented a new technique for measuring the adhesion strength of atmospheric ice during its growth. It uses wires aligned on the surface, on which ice accumulates, and measures the adhesion strength of ice to wires during ice growth using a force sensor. Using this technique, the adhesion strength of growing ice has been measured. The measurements were performed using an icing wind tunnel, under the conditions of liquid water content (LWC) form 0.3 to

2.4 g/m^3, air speeds of 10 and 20 m/s, and an air temperature of −10 °C.

The measurements showed that the adhesion strength significantly depended on time and it varied with LWC and air speed. The adhesion strength of growing ice decreases with either the increase of LWC or the increase of air speed at the early stage of atmospheric icing but the trend became the opposite after certain time.

There were two possible factors causing the various dependences of the adhesion strength of growing ice. One was the porosity. The other was the freezing process of growing ice, related to the ice temperature and the phase change from water to ice.

To investigate the effect of freezing process on the adhesion strength, we introduced a dimensionless number, Rt, which provided the reduction of the adhesion strength of growing ice from that of the frozen ice due to the freezing process. The analysis showed that the freezing process caused the time dependence of the adhesion strength of growing ice. This effect was more pronounced in weakening the adhesion strength at the beginning of ice growth, but it gradually diminished with time. The effect of freezing process became more effective in weakening the adhesion strength with either the increase of LWC or the decrease of air speed.

To investigate the effect of porosity on the adhesion strength of growing ice, the measurements of the adhesion strength of frozen ice and the naked eye observation of the porosity were performed.

54

Comparison of those results showed that the LWC and air speed

dependences of the adhesion strength were interpreted as those

dependences of the porosity. The porosity was, in contrast to the

freezing effect, independent of time.

The difference of the dependencies on time, LWC, and air speed

between the freezing process and porosity factors explained the

complex trends that the adhesion strength decreases with either the

increase of LWC or the increase of air speed at the early stage of

atmospheric icing but the trend became the opposite after certain

time.

3.6 Appendix: Nomenclature

LWC = liquid water content in air

Rt = normalized adhesion strength of growing ice by frozen ice.

3.7 References

Druez,J., D. D. Nguyen, and Y. Lavoie (1987), Mechanical Properties of

       Atmospheric Ice, Cold Region Science and Technology, 13, 67-74.

Javan-Mashmool, M., C. Volat, and M. Farzaneh (2006), A new method for

       measuring ice adhesion strength at an ice-substrate interface,

       Hydrol. Process. 20, 645-655.

Lozowski, E. P., M Oleskiw, R. Z. Blackmore, and A. Karev, L. Kolar,

       and M. Frzanch (2005) Spongy Icing Revisited: Measurements of

Ice Accretion Liquid Fraction in Two Wind Tuunels, The 43rd AIAA

Aerospace Siences Meeting and Exhibit, Reno, NV, 10-13 January

2005.

Petrenko, V. F. and R. W. Whitworth (1999). Physics of Ice. Oxford

University Press: Oxford.

3.8 Figure Captions
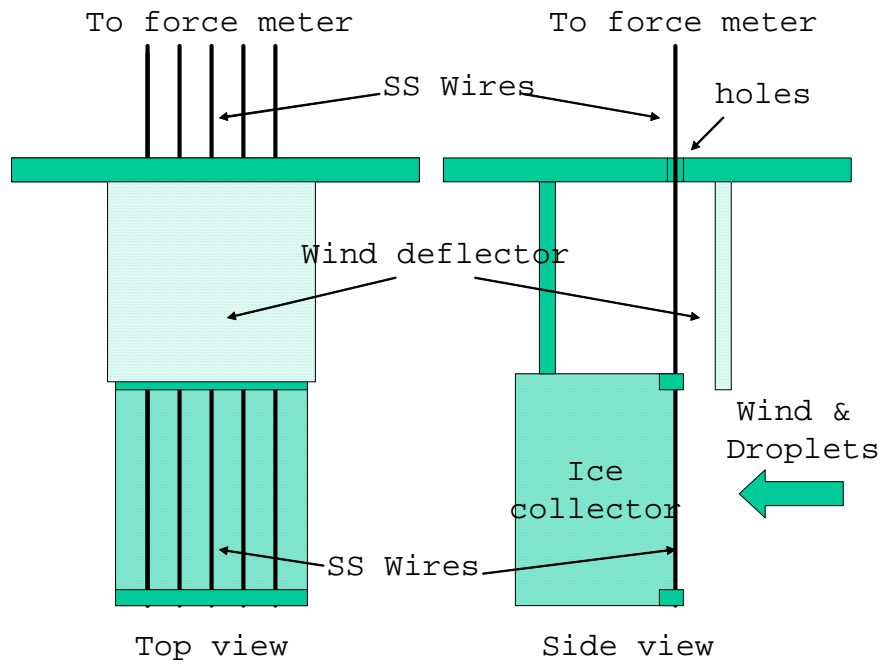
Figure 1. An illustration of experimental setup for the adhesion strength measurements.
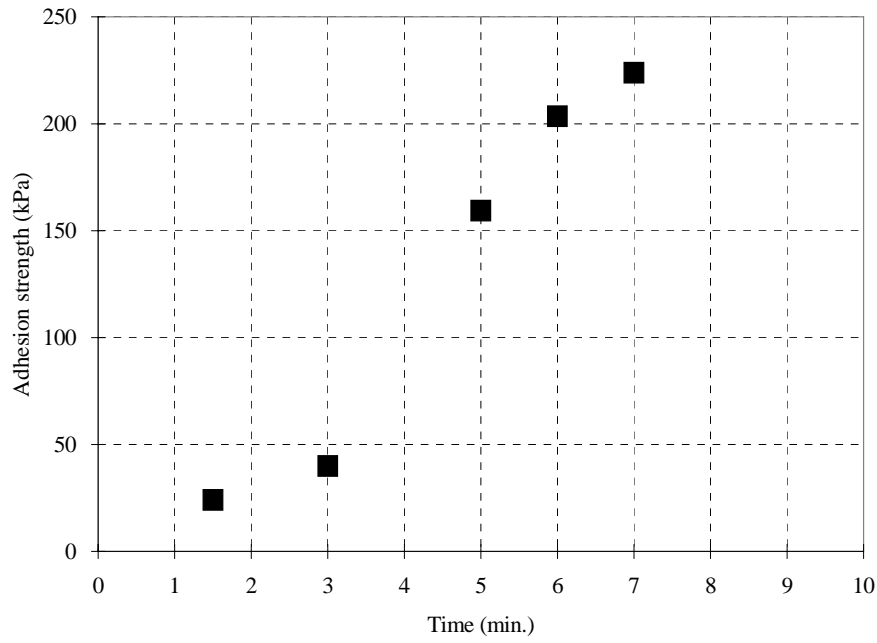
Figure 2. Adhesion strength of growing ice as a function of time. LWC of 1.1 +/- 0.3 g/m^3, an air speed of 20 m/s, and a temperature of -10 $^{\circ}$C.
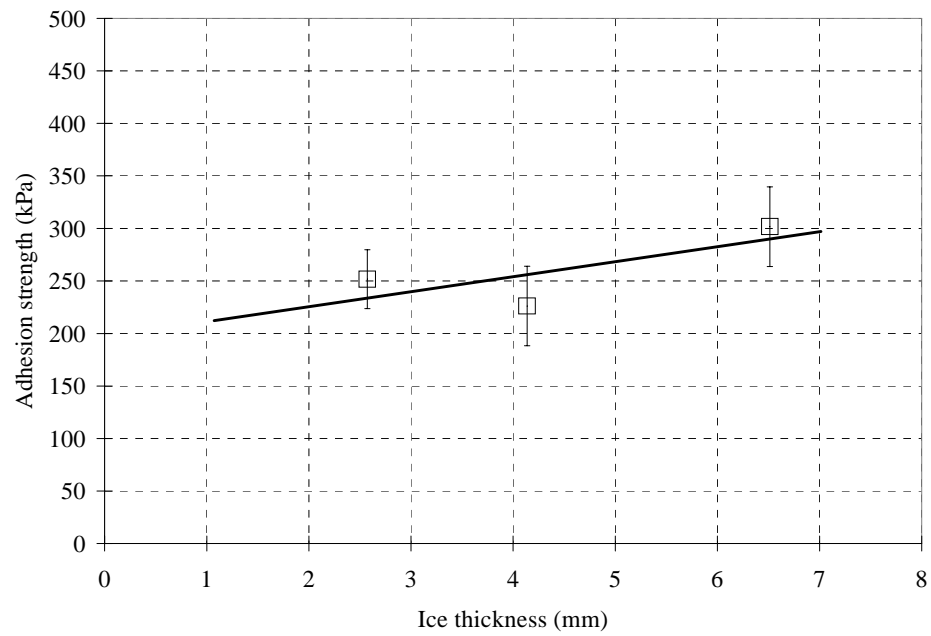
Figure 3. Adhesion strength of frozen ice as a function of ice thickness. The fit regression line is also shown. The conditions are the same as in Figure 2.

Figure 4. Dimensionless parameter Rt of growing ice as a function of time. The trend line is also shown. The conditions are the same as in Figure 2.

Figure 5. Adhesion strength of growing ice as a function of time for different LWC. Air speed of 20 m/s and temperature of -10 $^{\circ}$C.

Figure 6. Adhesion strength of frozen ice as a function of ice thickness for different LWC. The conditions are the same as in Figure 5.
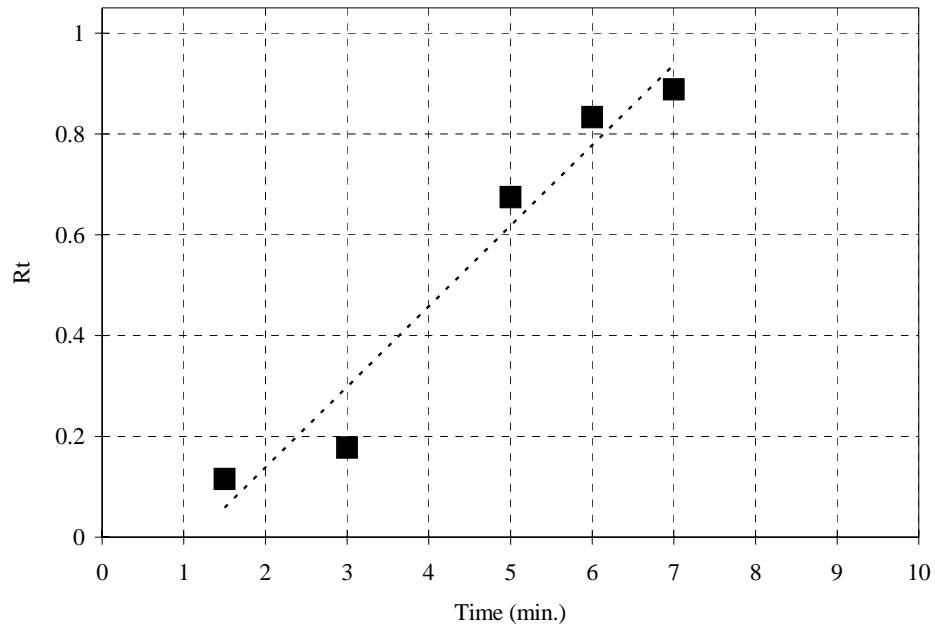
Figure 7. Dimensionless parameter Rt of growing ice as a function of time for different LWC. The trend lines are also shown. The conditions are the same as in Figure 5.
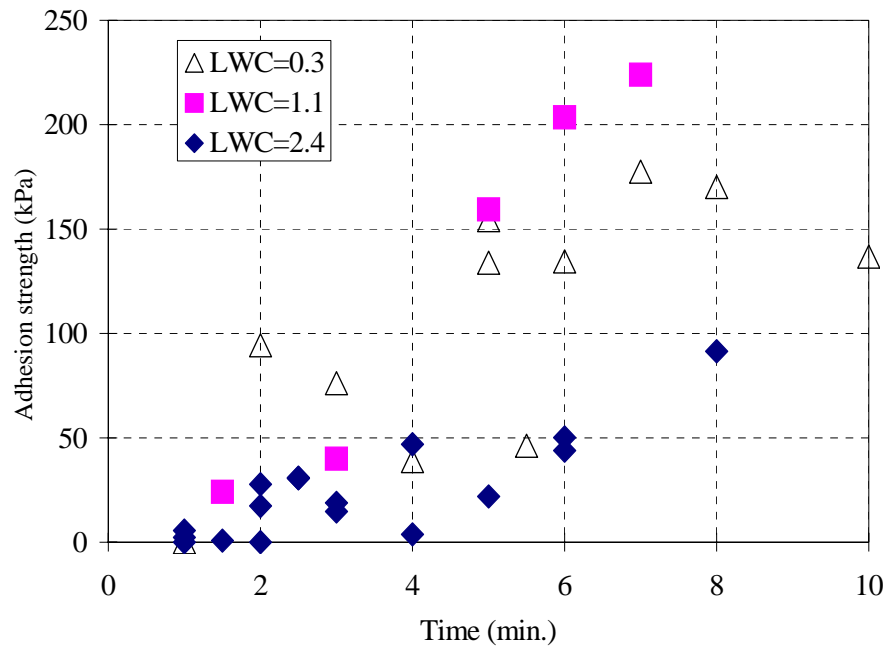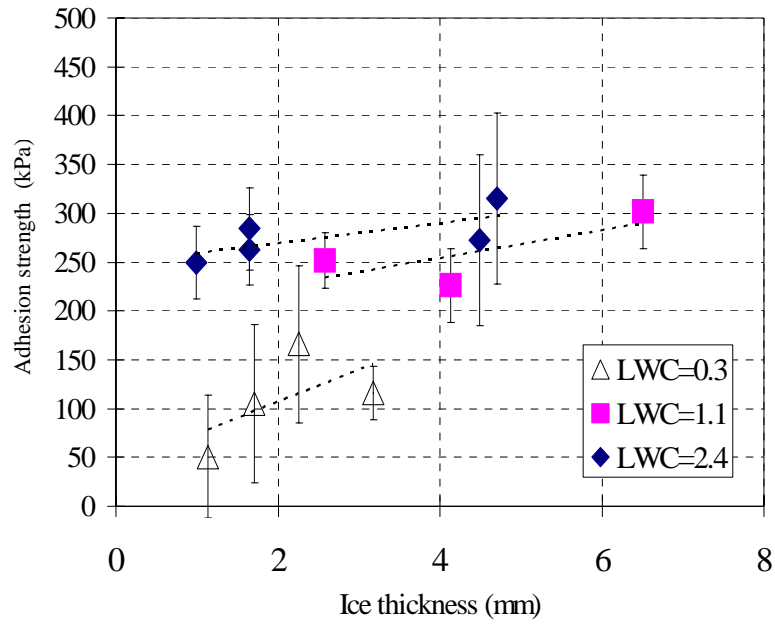
Figure 8. Adhesion strength compared between growing ice and frozen ice. LWC is 0.3 g/m^3.

Figure 9. Adhesion strength of growing ice as a function of time for

    different air speed of 20 m/s (LWC=1.1 g/m3) and 10 m/s (LWC=2.4

    g/m^3) at temperature of -10 ^{o}C.

Figure 10. Adhesion strength of frozen ice as a function of ice

    thickness for different air speeds. . The conditions are the same
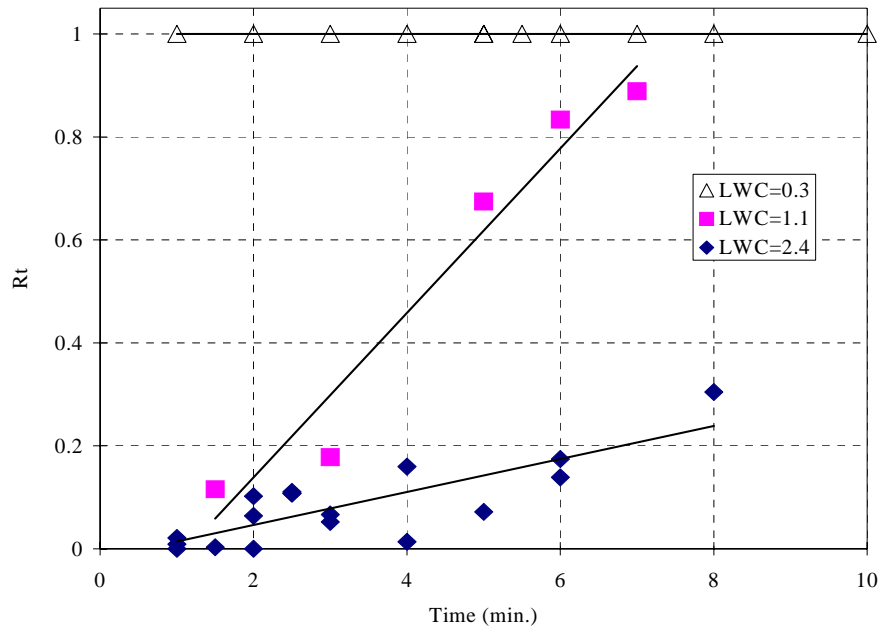
    as in Figure 5.

Figure 11. Dimensionless parameter Rt of growing ice as a function of

    time for different air speeds. The trend lines are also shown.

    The conditions are the same as in Figure 5.

Figure 12. A schematic picture of the adhesion strength of growing

    atmospheric ice as a function of time for different LWC. LWC =

    0.3, 1.1, 2.4 g/m^3

Fig.1

To force meter   To force meter

SS Wires   holes

Wind deflector

Wind &
Droplets

Ice
collector

SS Wires

Top view   Side view

Figure 1. An illustration of experimental setup for the adhesion strength measurements.

Fig.2

Figure 2. Adhesion strength of growing ice as a function of time. LWC of 1.1 +/- 0.3 g/m^3, an air speed of 20 m/s, and a temperature of -10 $^{\circ}$C.

Fig.3

Figure 3. Adhesion strength of frozen ice as a function of ice thickness. The fit regression line is also shown. The conditions are the same as in Figure 2.

Fig.4

Figure 4. Dimensionless parameter Rt of growing ice as a function
of time. The trend line is also shown. The conditions are the same
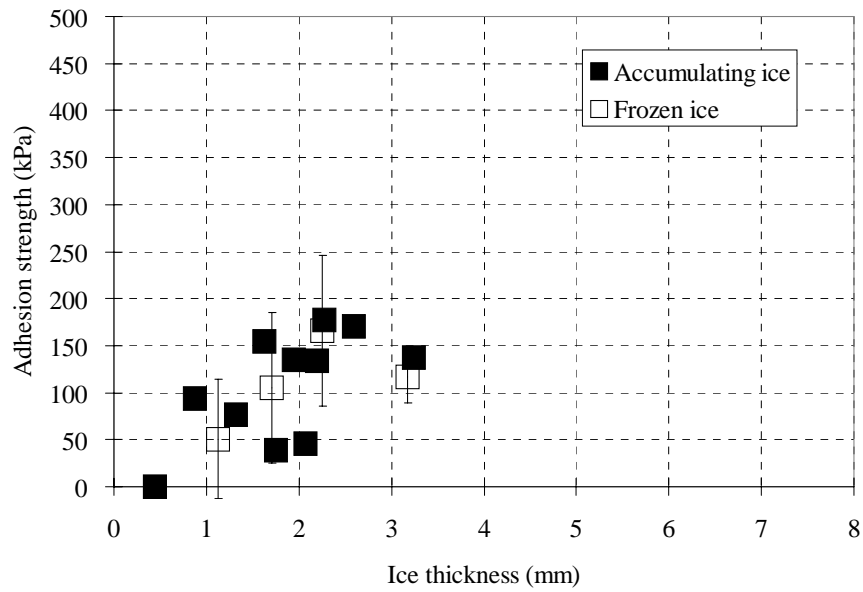as in Figure 2.

Fig.5

Figure 5. Adhesion strength of growing ice as a function of time for different LWC. Air speed of 20 m/s and temperature of -10 $^{\circ}$C.

Fig.6

Figure 6. Adhesion strength of frozen ice as a function of ice thickness for different LWC. The conditions are the same as in Figure 5.

Fig.7

Figure 7. Dimensionless parameter Rt of growing ice as a function

of time for different LWC. The trend lines are also shown. The

conditions are the same as in Figure 5.

Fig. 8

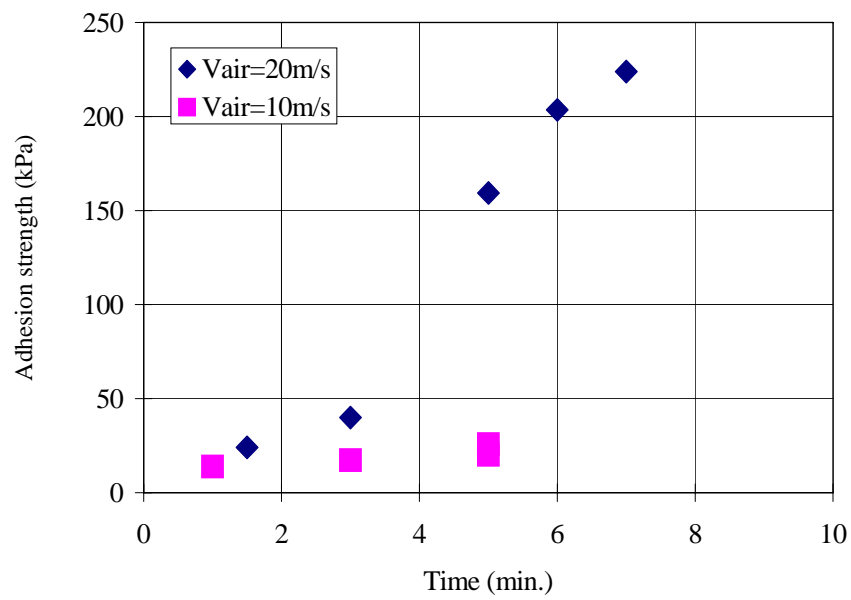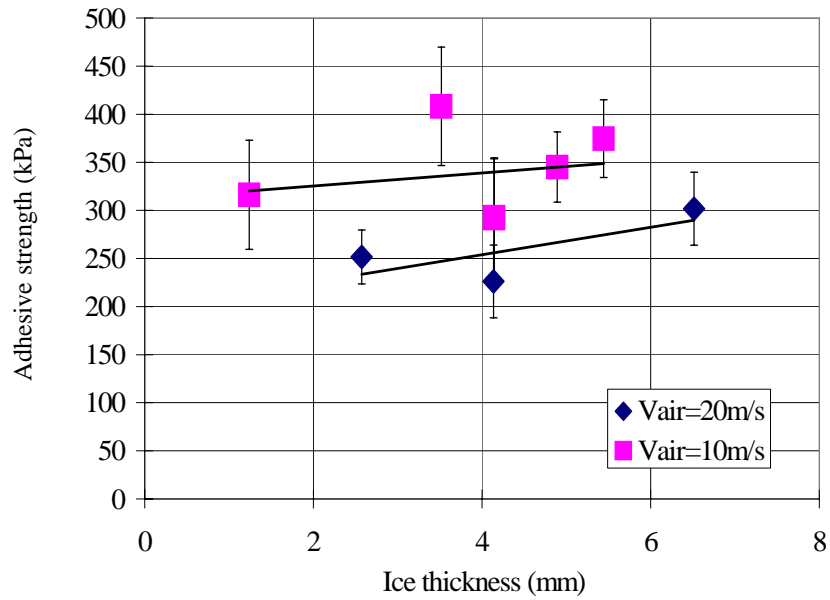Figure 8. Adhesion strength compared between growing ice and frozen ice for 0.3 g/m^3.

Fig. 9

Figure 9. Adhesion strength of growing ice as a function of time for different air speed of 20 m/s (LWC=1.1 g/m3) and 10 m/s (LWC=2.4 g/m3) at temperature of -10 $^{\circ}$C.

Fig.10

Figure 10. Adhesion strength of frozen ice as a function of ice thickness for different air speeds. . The conditions are the same as in Figure 5.
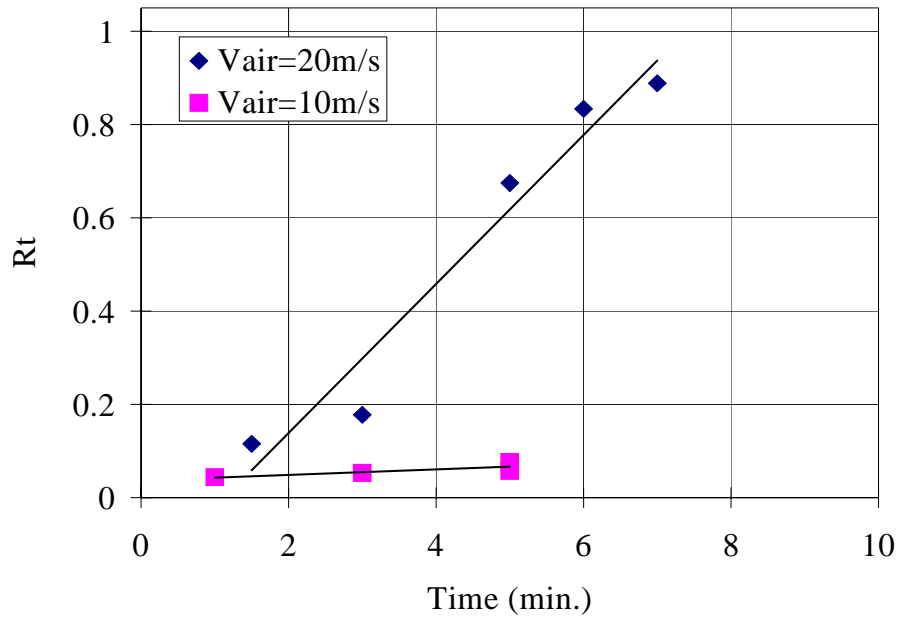
Fig. 11

Figure 11. Dimensionless parameter Rt of growing ice as a function

of time for different air speeds. The trend lines are also shown.

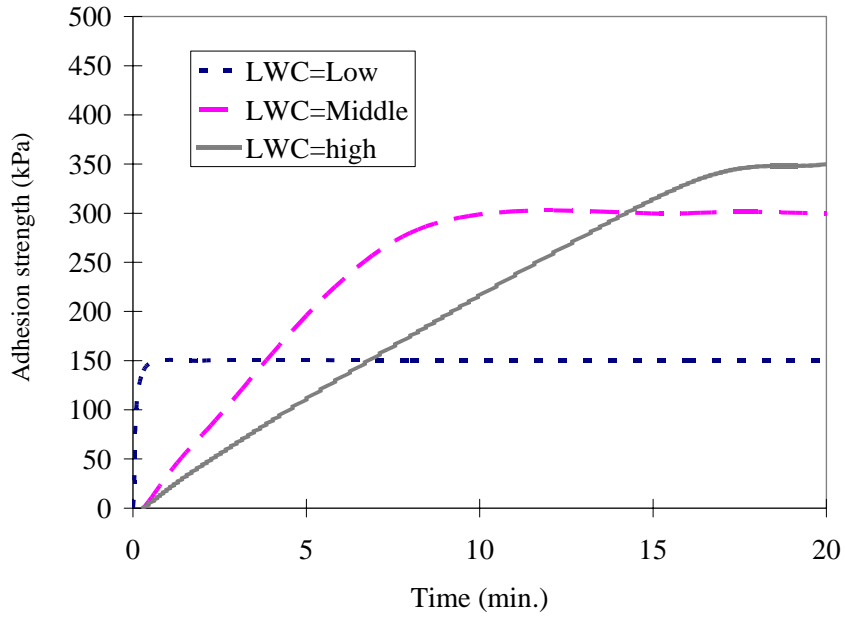The conditions are the same as in Figure 5.

Fig. 12

Figure 12. A schematic picture of the adhesion strength of growing atmospheric ice as a function of time for different LWC. The used experimental conditions: LWC=0.3, 1.1, and 2.4 g/m^3, temperature = −10 °C, air speed = 20 m/s.

4 ACKNOWLEDGMENTS